

THESIS FOR THE DEGREE OF LICENTIATE OF ENGINEERING

Multi-Gigabit Radio System Demonstrators for Next Generation Mobile Networks

Jingjing Chen



Microwave Electronics Laboratory
Department of Microtechnology and Nanoscience
CHALMERS UNIVERSITY OF TECHNOLOGY
Gothenburg, Sweden 2015

Multi-Gigabit Radio System Demonstrators for Next Generation Mobile Networks

Jingjing Chen

© Jingjing Chen, 2015

Technical Report MC2-307
ISSN 1652-0769

Microwave Electronics Laboratory
Department of Microtechnology and Nanoscience – MC2
Chalmers University of Technology
SE-412 96 Goteborg, Sweden
Phone: 46 (0) 31 772 10 00

Printed by Chalmers Reproservice
Gothenburg, Sweden 2015

“You don't stop running because you get old, you get old because you stop running.”

— Christopher McDougall, *Born to Run*

Abstract

Driven by the exponential growth in mobile broadband subscriptions and mobile data traffic, transport capacity of mobile networks has to be enhanced accordingly, including wireless backhaul and the emerging fronthaul networks. Utilizing wide bandwidth is the most straightforward way to capacity upgrade. Millimeter-wave frequency bands with large available bandwidth offer the opportunities to realize high capacity wireless links. However, there are challenges associated with the radio link implementation. For example, wide bandwidth is required for components like low noise amplifiers, power amplifiers, modulators and demodulators (modems). Another challenge is the signal quality degradation due to high frequency impairments.

The solutions presented in the thesis are applicable to implementations based on commercially available hardware. Multi-gigabit modems are proposed using simple modulation differential quadrature phase shift keying (DQPSK), which do not need carrier recovery and power hungry mixed signal devices. To improve spectral efficiency, a 16-QAM modem is designed with optimized hardware efficiency. This in turn relaxes the demand on the sampling rate of analog to digital converters (ADC) and the resource requirement on digital signal processing. As proof-of-concept demonstration, DQPSK modems are implemented and verified at 2.5 and 5 Gbps. A 5 Gbps radio system based on the hardware efficient 16-QAM modem is also demonstrated at 70/80 GHz (E-band). The presented modems and systems address challenges in applying wide bandwidth/high symbol rate to realizing high capacity. Moreover, it defines the baseline for further capacity enhancement when combined with high spectral efficiency techniques.

Besides the mobile backhaul application, high capacity wireless links are required to support the mobile fronthaul as a new network segment, which connects a centralized baseband pool to distributed remote radio units. A data-rate adaptable DQPSK modem solution is proposed for digital wireless fronthaul to transmit multi-gigabit CPRI (common public radio interface). An E-band digital fronthaul link is implemented using this modem at 5 Gbps. To overcome the low bandwidth efficiency of the digital fronthaul, an analog fronthaul technology is introduced as an enabler for cost efficient and scalable fronthaul networks. An analog fronthaul link is demonstrated at E-band complemented with phase noise mitigation for 64-QAM LTE transmission.

Keywords: mobile backhaul, fronthaul, centralized baseband, millimeter-wave transmission, E-band, point-to-point radio, modem, multi-gigabit, DQPSK, differential coding, 16-QAM, FPGA, phase noise mitigation.

List of Publications

Appended papers

The thesis is based on the following papers:

- [A] Z. He, **J. Chen**, Y. Li, H. Zirath, “A novel FPGA-based 2.5Gbps DQPSK modem for high capacity microwave radios,” *International Conference of Communications (ICC2010)*, Cape Town, May, 2010.
- [B] **J. Chen**, Z. He, L. Bao, C. Svensson, Y. Li, S. Gunnarsson, C. Stoj, H. Zirath, “10 Gbps 16QAM transmission over a 70/80 GHz (E-band) radio test-bed,” *European microwave conference (EuMC)*, Amsterdam, October, 2012.
- [C] Z. He, **J. Chen**, C. Svensson, L. Bao, A. Rhodin, Y. Li, J. An, H. Zirath, “A hardware efficient implementation of a digital baseband receiver for high capacity millimeter-wave radios,” accepted for publication in *IEEE Transactions on Microwave Theory and Techniques*.
- [D] **J. Chen**, Z. He, Y. Li, T. Swahn, H. Zirath, “A data-rate adaptable modem solution for millimeter-wave wireless fronthaul networks,” *International Conference of Communications (ICC2015) Workshop*, London, June, 2015.
- [E] **J. Chen**, B. E. Olsson, A. Persson, J. Hansryd, “Experimental demonstration of RF pilot-based phase noise mitigation for millimeter-wave systems,” *Vehicular Technology Conference (VTC2014-Fall)*, Vancouver, September, 2014.
- [F] **J. Chen**, B. E. Olsson, J. Hansryd, I. Gerszberg, “Demonstration of analog millimeter-wave fronthaul for 64-QAM LTE transmission,” submitted to *Vehicular Technology Conference (VTC2015-Fall)*, Boston, September, 2015.

Other papers

The following papers have been published but are not included in the thesis. The content partially overlaps with the appended papers or is out of the scope of the thesis.

- [a] J. Hansryd, **J. Chen**, Y. Li, “A simple DBPSK modem based on high-speed logical gates for a 70/80 GHz GbE microwave link,” *Vehicular Technology Conference (VTC 2010-Spring)*, Taipei, May, 2010.
- [b] Z. He, W. Wu, **J. Chen**, Y. Li, H. Zirath, “An FPGA-based 5Gbit/s D-QPSK modem for E-band point-to-point radios,” *European microwave conference (EuMC)*, Manchester, October, 2011.
- [c] Z. Ghebretensae, K. Laraqui, S. Dahlfort, **J. Chen**, Y. Li, J. Hansryd, F. Ponzini, L. Giorgi, S. Stracca, A.R. Pratt, “Transmission solutions and architectures for heterogeneous networks built as C-RANs,” *International ICST Conference on Communications and Networking in China (CHINACOM)*, Kunming, August, 2012.
- [d] M. Bao, **J. Chen**, R. Kozhuharov, H. Zirath, “A high speed power detector for D-band communication,” *IEEE Transactions on Microwave Theory and Techniques*, vol. 62, no. 7, pp. 1515-1524, July, 2014.

Abbreviations

3G/4G/5G	Third/Fourth/Fifth generation of mobile communications technology
ADC	Analog to digital converter
ASK	Amplitude shift keying
AWG	Arbitrary waveform generator
BBU	Baseband unit
BER	Bit error rate
BSC	Base station controller
BPF	Band pass filter
CDR	Clock and data recovery
C-RAN	Centralized radio access network
CR	Carrier recovery
CPRI	Common public radio interface
DAC	Digital to analog converter
DBPSK	Differential binary phase shift keying
DDCR	Decision-direct carrier recovery
DQPSK	Differential quadrature phase shift keying
DSP	Digital signal processing
EVM	Error vector magnitude
FDD	Frequency division duplexing
FPGA	Field programmable gate array
GbE	Gigabit Ethernet
CoMP	Coordinated multi-point transmission
IF	Intermediate frequency
LO	Local oscillator
LPF	Low pass filter
LTE	Long-term evolution
LUT	Look-up table
MIMO	Multiple input and multiple output
Modem	Modulator and demodulator
MSC	Mobile switching center
OFDM	Orthogonal frequency division multiplexing
OOK	On-off keying
PCB	Printed circuit board
PAPR	Peak-to-average power ratio
PLL	Phase-locked loop
PRBS	Pseudo random binary sequence
PSPR	Pilot-to-signal power ratio
PPL	Parallel prefix layer

PPN	Parallel prefix network
QAM	Quadrature amplitude modulation
QPSK	Quadrature phase shift keying
RAT	Radio access technology
RBS	Radio base station
ROM	Read-only memory
RF	Radio frequency
RRU	Remote radio unit
STR	Symbol timing recovery
SNR	Signal-to-noise ratio

Contents

- Abstract** **v**

- List of Publications** **vii**

- Abbreviations** **ix**

- 1 Introduction** **1**
 - 1.1 Background** **1**
 - 1.2 Thesis scope and outline** **3**

- 2 Challenges and Motivation** **5**
 - 2.1 Challenges in future mobile networks** **5**
 - 2.1.1 Mobile network evolvement** **5**
 - 2.1.2 Introduction to mobile fronthaul** **6**
 - 2.1.3 Capacity challenge in microwave transmission** **8**
 - 2.2 Capacity enhancement** **8**
 - 2.2.1 Millimeter-wave frequency bands** **9**
 - 2.2.2 Spectrally efficient technologies** **10**
 - 2.3 Implementation challenges in high data rate systems** **11**
 - 2.4 Overview of realized multi-gigabit demonstrators** **12**
 - 2.5 Challenges in wireless fronthaul networks** **14**
 - 2.6 Realized fronthaul demonstrators** **14**

- 3 Multi-Gigabit Modem and System Demonstrators** **15**
 - 3.1 Differential QPSK modulation** **15**
 - 3.1.1 Comparison of QPSK and DQPSK** **15**
 - 3.1.2 DQPSK modulator** **16**
 - 3.1.3 Differential encoder** **16**

3.2	Multi-gigabit DQPSK modems with non-coherent detection	18
3.2.1	FPGA-based DQPSK modulator.....	18
3.2.2	DQPSK demodulator implementation	19
3.2.3	Multi-rate DQPSK modem implementation	20
3.3	Spectrally efficient modems with coherent detection	23
3.3.1	Synchronization in coherent detection	24
3.3.2	Overview of published spectrally efficient solutions.....	25
3.3.3	Implementation of a hardware-efficient 16-QAM demodulator	25
3.4	Multi-gigabit systems	30
3.4.1	5/10 Gbps system demonstrators at 70/80 GHz (E-band)	30
4	Millimeter-wave Fronthaul Demonstrators.....	33
4.1	Digital fronthaul	33
4.1.1	Fixed-rate demonstrator	34
4.1.2	Adaptable data-rate demonstrator.....	35
4.2	Analog fronthaul	36
4.2.1	Advantages and challenges	37
4.3	High frequency impairments mitigation	38
4.3.1	The principle of phase noise mitigation.....	39
4.3.2	Performance optimization	41
4.3.3	Experimental demonstration over millimeter-wave.....	41
4.4	Analog fronthaul demonstrator	43
4.4.1	Implementation of analog fronthaul at 70/80 GHz	43
4.4.2	Evaluation of transmission performance	44
4.4.3	Fronthaul link characterization	46

5	Conclusions and Future Outlook.....	49
	5.1 Conclusions	49
	5.2 Opportunities at 140-GHz band	50
	Acknowledgments.....	51
	References	53

Chapter 1

Introduction

1.1 Background

Today, the number of mobile-connected devices has exceeded the number of people on Earth and it is growing faster than the world's population [1]. As predicted by an Ericsson forecast in [2], the number of mobile subscriptions will be over 9 billion by the end of 2019, of which more than 80% will have mobile access to the Internet (mobile broadband). We are on a journey to a networked society where information access and sharing will be possible anywhere at any time for anyone and anything. Future mobile networks will extend connectivity beyond people for device-to-device (D2D) communication and machine-type communication (MTC). Consequently, beyond 2020 mobile networks are expected to deliver a 1000 times increase in traffic capacity compared to the 4G networks of today [3]. Driven by the mobile data explosion, the mobile networks continue to evolve into 5G and the capacity of mobile backhaul networks has to be enhanced accordingly.

The mobile backhaul network connects radio base stations (RBSs) to mobile switching centers of the core network. As illustrated in Fig. 1.1, the backhaul network can be divided into two parts: the low radio access network (LRAN) and the high radio access network (HRAN) [4]. The HRAN, also referred to as the metro network, aggregates traffic from a number of LRANs. Typically, it is built by optical fibers due to high transport capacity and microwave radios are used for redundancy. The LRAN provides connectivity from the RBSs to the HRAN up to a few kilometres, which is known as the last mile access. Point-to-point microwave technology is dominant in the LRAN, as shown in Fig. 1.2, connecting 50% of the installed RBSs worldwide [2].

Compared to optical fiber links, microwave backhaul is a cost-efficient and flexible alternative although the capacity of microwave links is limited mainly due to regulations of the channel bandwidth. However, advances in mobile technologies always trigger an increase of the backhaul capacity. For example, multi-gigabit capacity is expected to backhaul base stations using LTE (long-term evolution) advanced technology by 2019 (Fig. 1.3) [2]. Microwave transmission must overcome this capacity barrier in order to be future proof.

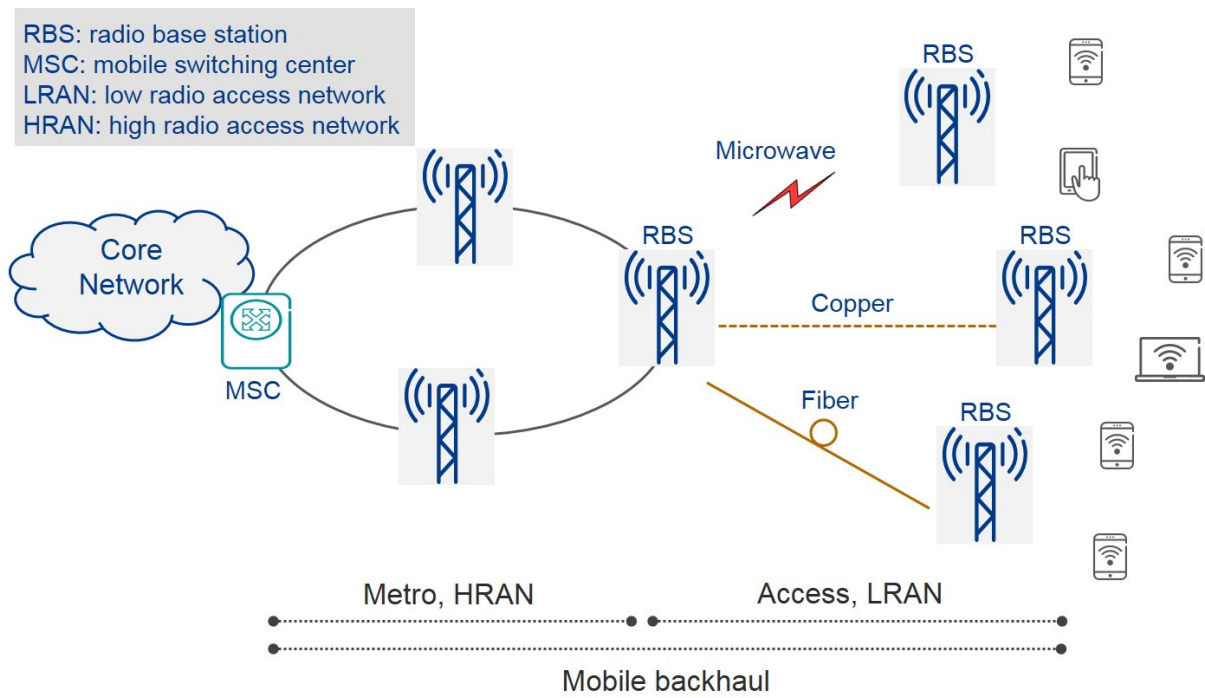
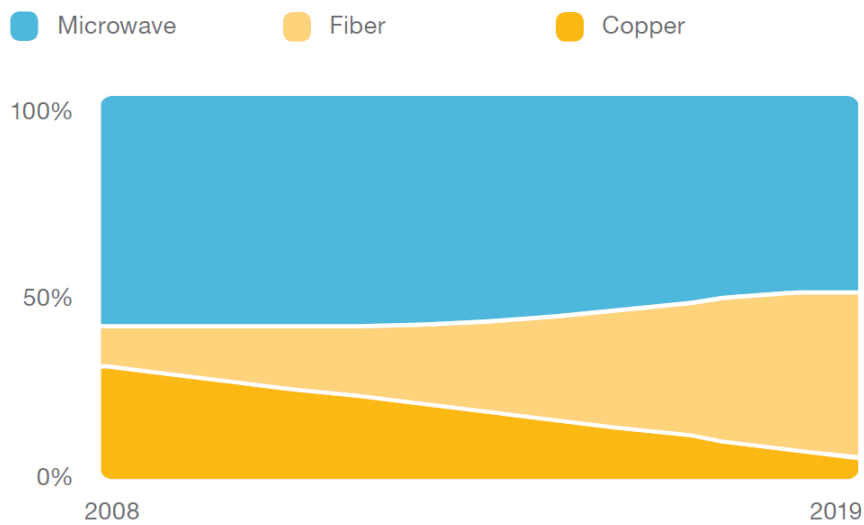


Figure 1.1: Mobile backhaul network.



Source: Ericsson (2014)

Figure 1.2: Market share of different backhaul technologies [2].

3G operator introducing LTE in 2013 evolving to LTE advanced

	2013	2016	2019
80% of sites	50 Mbps	180 Mbps	270 Mbps
20% of sites	180 Mbps	540 Mbps	900 Mbps
Few % of sites	360 Mbps	900 Mbps	1.8 Gbps

Source: Ericsson (2014)

Figure 1.3: Backhaul capacity forecast of LTE and LTE advanced base station sites [2].

1.2 Thesis scope and outline

As indicated by Shannon theorem, utilizing a wider channel can proportionally increase the capacity of a transmission link. Millimeter-wave (mm-wave) bands with tens of GHz bandwidth available open up opportunities for wireless links to reach fiber-like capacity. However, there are challenges associated with the radio link implementation. For example, wide bandwidth modulators and demodulators (modems) are needed, therefore advanced digital modulation techniques are not always applicable today due to hardware limitations and cost/power issues. Consequently, it is practical to realize analog designs in some cases as a complement to digital modems. It is not only the spectral efficiency that is important to consider, but also design factors including system complexity, cost issues, and requirements on hardware.

The scope of the thesis is to investigate high data rate system solutions at mm-wave bands, which shall be feasible based on available and accessible hardware. Driven by a strong interest from the industry, a special focus has given to the 70/80 GHz frequency band (E-band) which besides offering 10 GHz bandwidth is regulated worldwide for commercial use with a light licensing model.

Chapter 2 discusses the associated challenges with high data rate and high carrier frequency in greater detail. Besides mobile backhaul, the emerging fronthaul network is introduced as a new segment in the evolved mobile network. The fronthaul network also requires high data rate transmission links, but with additional requirements. An overview of the realized solutions in this thesis is presented to address some of the challenges in backhaul and fronthaul networks. In chapter 3, multi-gigabit modem solutions are described based on differential quadrature phase shift keying (DQPSK) modulation, which are implemented in a cost-and power-efficient manner. The DQPSK modems are demonstrated at fixed rate 2.5 and 5 Gbps, as well as up to 10 Gbps as a data-rate adaptable solution, thanks to a novel differential coding scheme. Moreover, a 16-QAM baseband receiver is proposed with combined analog and digital operations for being hardware efficient. The receiver is demonstrated with an E-band front-end at 5 Gbps. Chapter 4 introduces two distinct solutions tailored for fronthaul application. One of them supports multi-rate digital CPRI transmission

up to 10 Gbps and is dedicated to conventional digital fronthauls. Another solution is designed as a bandwidth efficient fronthaul technology, named analog fronthaul. An E-band analog fronthaul link is demonstrated for 64-QAM LTE transmission. In the last chapter, future research opportunities and challenges are identified towards 100 Gbps capacity at beyond 100 GHz carrier frequency.

Chapter 2

Challenges and Motivation

2.1 Challenges in future mobile networks

2.1.1 Mobile network evolution

The exponential growth of mobile data traffic imposes significant demands on mobile networks. Network densification is an efficient tool for improved capacity and coverage, where low power small cells are deployed as a complement to existing macro cells to form what is known as a heterogeneous network. The overall network capacity increase comes at a price of growing cost for mobile operators. As reported by China Mobile, 60% of the total cell site cost is operational expense (OPEX) compared to 40% of initial capital expense (CAPEX) of the new equipment over a 7-year period, and approximately 20% of the overall site cost is power consumption [5]. Since a large number of small cells are foreseen to be installed to meet the demanding end-user expectations, mobile operators are looking for solutions to lower the operational cost. Centralized baseband architecture, also referred to as the centralized radio access network (C-RAN) has been proposed accordingly.

Traditional base stations are equipped with baseband units and radio units at each cell site. However, in a centralized baseband architecture, baseband units (BBU) are placed in a central office or in a BBU pool for centralized processing and management, and only the remote radio units are located next to the antennas at the cells sites, as illustrated in Fig. 2.1. Site configuration as such is applicable to the deployment of both small cells and macro cells, where small cells typically have one RRU, while macro cells would need more RRUs. The cells sites are simplified as compared to the traditional integrated ones. Therefore, both space requirement and power consumption can be reduced to lower the operational cost. Moreover, centralized baseband processing enables advanced coordination among the cells for interference mitigation using coordinated multi-point transmission (CoMP). By balancing the data traffic among the cells, it is possible to optimize capacity for individual users so that spectrum/power efficiency can be improved as well as the user experience.

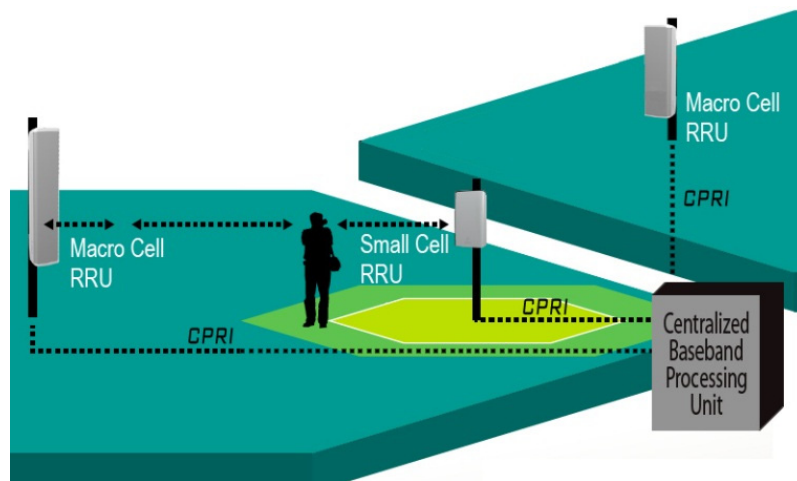


Figure 2.1: Small cells and macro cells in a heterogeneous network are deployed using remote radio units (RRU), connected to a centralized baseband processing unit through CPRI links [D].

2.1.2 Introduction to mobile fronthaul

A new network segment is created by the introduction of a centralized baseband processing, the so called fronthaul network which connects the BBU to distributed RRUs at the cell sites. Fig. 2.2 describes the difference between the fronthaul and the backhaul in a mobile network. The centralized baseband architecture offers high network performance and is believed to be low cost, provided that the fronthaul network can be realized in an efficient way for dense deployment. Besides, a fronthaul network should support Gbps capacity, low latency and multiple radio access technologies (RAT). The most used interface between the BBU and the RRU is known as common public radio interface (CPRI), which transfers digitized radio signals as oversampled I/Q data. The CPRI standard specifies data rates up to 10 Gbps depending on the configured access technology, carrier bandwidth and so on. The allowed bit-error-rate (BER) is limited to maximum 10^{-12} for the CPRI interface [6]. To ensure quality of service, LTE-advanced [7] requires the maximum round-trip delay to be of about $400 \mu\text{s}$ including both transmission delay and fronthaul equipment processing delay [8]. Although the CPRI standard does not specify the transmission medium, optical fibers have been used almost exclusively as the fronthaul link technology because of the demanding CPRI data rate. For example, to support one LTE sector with 20 MHz bandwidth and 2x2 multiple input multiple output (MIMO) configuration, CPRI data rate of 2.5 Gbps is required.

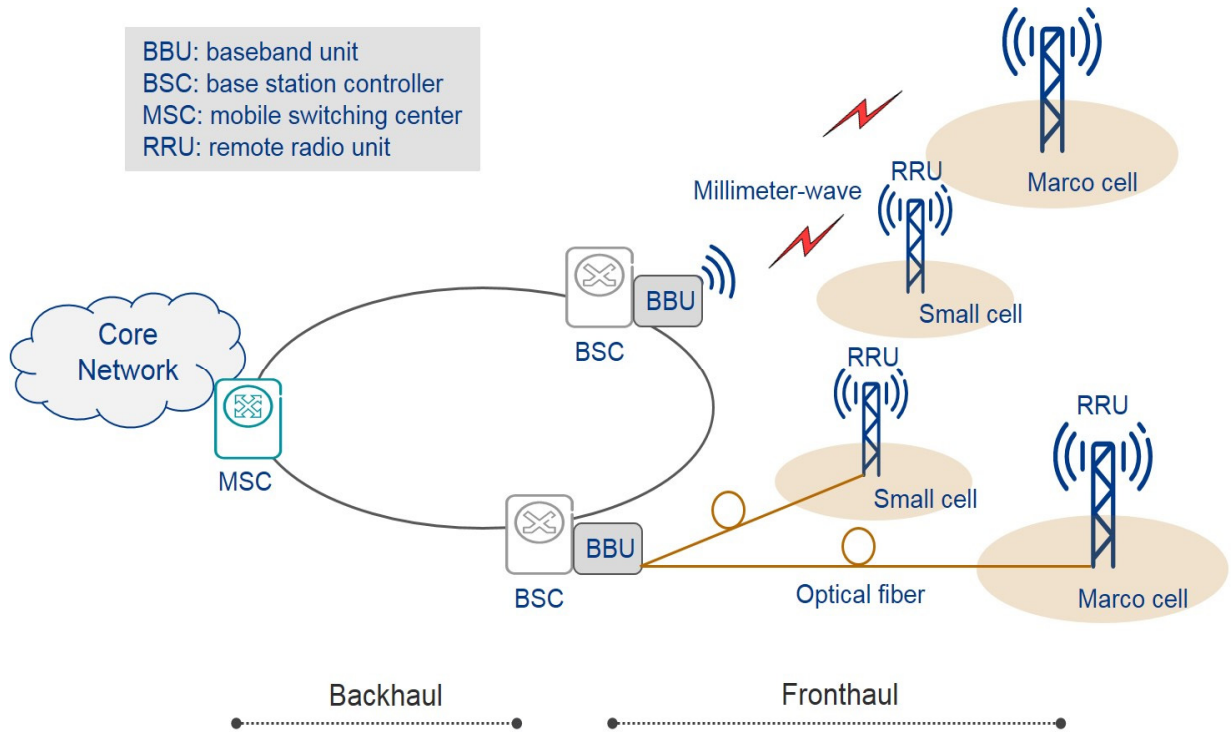


Figure 2.2: Fronthaul and backhaul in a mobile network.

2.1.3 Capacity challenge in microwave transmission

Fiber optical communication technology is very often the first choice for high data rate transmission. However, due to cost and availability issues, installing fibers is not always viable. Because of these limitations, high speed wireless technologies are expected to be an alternative. Point-to-point microwave radio with more than km reach is the most promising alternative, despite the capacity gap compared to fiber optics, as indicated in Fig. 2.3.

However, the capacity challenge has been pushing microwave technologies up to mm-wave frequency bands (e.g. 70/80 GHz) to realize fiber-competitive capacities.

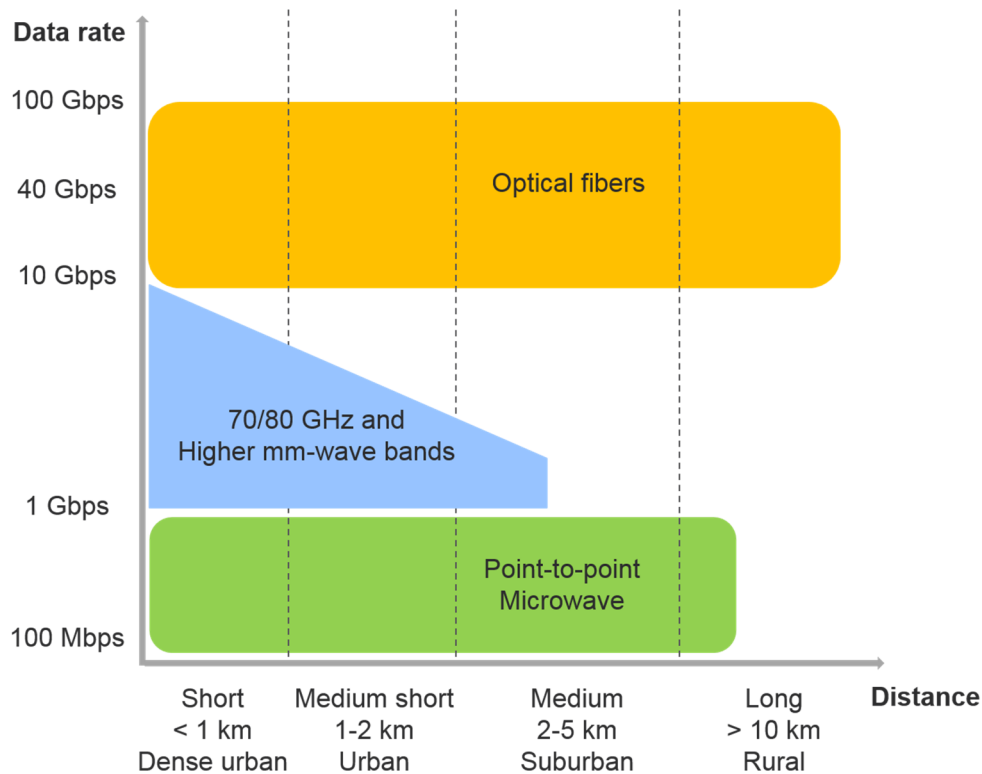


Figure 2.3: Comparison of microwave radios, millimeter-wave radios, and optical fibers in terms of data rate and link distance (the figure is modified based on Figure 7 in [9]).

2.2 Capacity enhancement

In principle, there are two ways to increase transmission capacity, applicable to both wireless and wired channels: by increasing the operational bandwidth and by efficiently using the available channel bandwidth.

Radio technology is more flexible than optical fiber links and allows a fast installation. However, it is necessary to allocate frequency bands for radio transmission so that adjacent users/channels do not disturb each other. The frequency allocation is controlled by regulatory instances, such as Federal Communications Commission (FCC) in the US and (European Telecommunications Standards Institute (ETSI) in Europe. Another important aspect is the propagation characteristics, which limits the choice of frequency bands. Because radio waves are subject to atmospheric attenuation due to absorption by gases (e.g. O₂) and rain (H₂O), and there are peaks in absorption at certain frequencies to avoid for a longer transmission range.

2.2.1 Millimeter-wave frequency bands

The capacity of microwave radios is limited mainly due to the very narrow channels regulated in conventional microwave bands (6 – 42 GHz), which are typically 28 MHz and 56 MHz in Europe [10]. The key for increasing capacity is to increase the bandwidth by using mm-wave frequency bands, in which large frequency spectrum is available to support high data rate wireless links.

Fig. 2.4 reveals a number of atmospheric windows centered around 80 GHz, 140 GHz, and 220 GHz, where the attenuation of radio waves is relatively low. Actually, the attenuation is higher than at lower frequencies which results in a shorter link distance. However, the short wavelength at high carrier frequency allows compact antennas with a small beam width, which increases the potential of frequency reuse for improved capacity and coverage. In addition, hardware size reduction makes installation of radio links easier on street-level in dense urban areas.

70/80 GHz often referred to as E-band is regulated from 71 – 76 GHz and 81 – 86 GHz with sufficient bandwidth to support Gbps operation and beyond. The E-band is available for commercial use in fixed services, and it is managed similarly worldwide with a light licencing model, allowing low spectrum cost and fast installation. The 90-GHz band (92 – 94 GHz) is not very practical due to its proximity to the military communication band (94 – 94.1 GHz). The next spectrum of interest is the 140-GHz band, which is allocated from 141 – 148.5 GHz. Besides, an 8-GHz wide allocation around 220 GHz (209 – 217 GHz) is available in the US for fixed services.

Because of the large available bandwidth, 70/80 GHz and 140-GHz bands at the atmospheric windows show a great potential for delivering multi-gigabit capacity over kilometer reach. In the thesis, 70/80 GHz is the main technology focus due to the commercial interest.

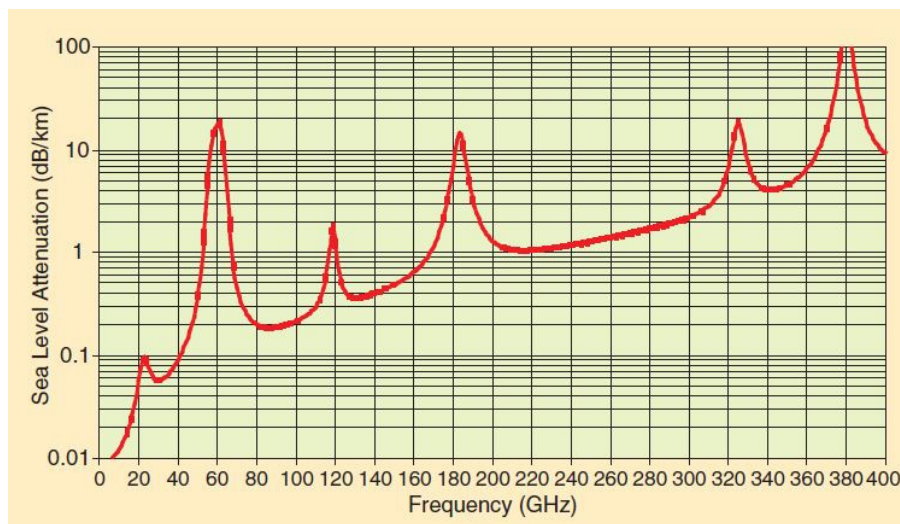


Figure 2.4: Atmospheric absorption as a function of frequency [9].

2.2.2 Spectrally efficient technologies

For a given channel, the data rate can be increased by improving spectral efficiency with high order modulations. The channel bandwidth sets the limit on the symbol rate, measured in symbols/s or baud, to be transmitted. The data rate R can be expressed as $R = S \cdot \log_2(M)$, where S is the symbol rate and M is the number of distinct symbols that can be sent. Taking Quadrature amplitude modulation (QAM) as an example, M -order QAM (M -QAM) modulation means $\log_2(M)$ number of bits are coded on each symbol. It is clear that increasing the modulation order M can deliver more data in the same bandwidth. Fig. 2.5 shows constellation diagrams of some common digital modulation schemes [11].

However, by moving to a higher order modulation, for a constant mean energy of the constellation, the points must be packed denser, and thus are more vulnerable to noise and interference. As a result, a higher order modulation suffers from a higher bit error rate (BER), or requires a higher signal-to-noise ratio (SNR) to maintain the same BER performance, as indicated in Fig. 2.6. Comparing QPSK to 8PSK, a 3 dB extra in SNR is required by coding one more bit per symbol, which corresponds to a 3 dB increase in receiver sensitivity. Moreover, a high order QAM signal typically has a high value of the peak-to-average power ratio (PAPR). To avoid signal distortion, the transmitter has to back off from the maximum output power to stay in the linear region with an amount corresponding to the increased PAPR. Hence, a lower output power is delivered for a higher order QAM. Consequently, the system gain is reduced as a penalty, which results in a shorter transmission distance and/or a lower availability of the wireless link.

Although the data rate increases by applying a high order modulation, the modulation shall be chosen dependent on the SNR of the system. In addition, for a realistic hardware implementation, requirements on phase noise and linearity of the radio transceivers shall also be considered.

On top of high order modulations, multi-carrier techniques can be employed to further increase the spectral efficiency and hence the data rate, such as polarization multiplexing and spatial multiplexing [10]. Multi-carrier techniques are outside the scope of the thesis, and will not be discussed in detail.

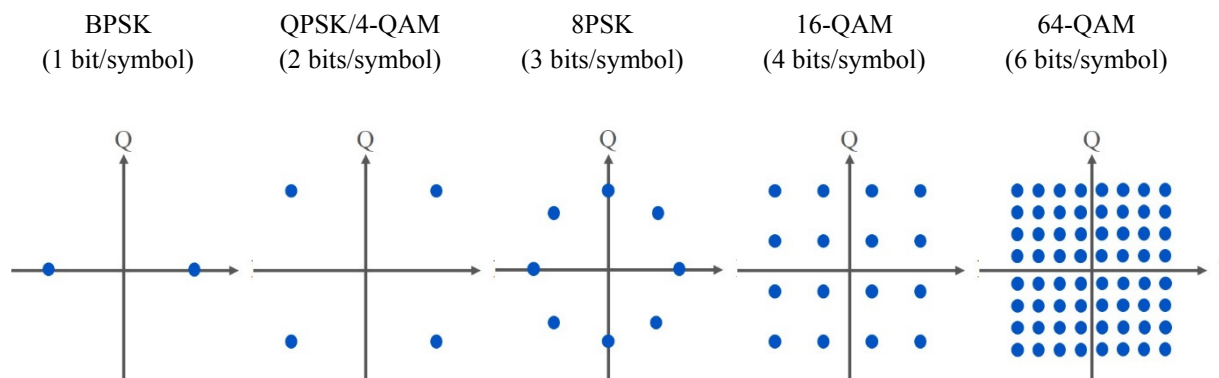


Figure 2.5: Constellation diagrams of common modulation schemes.

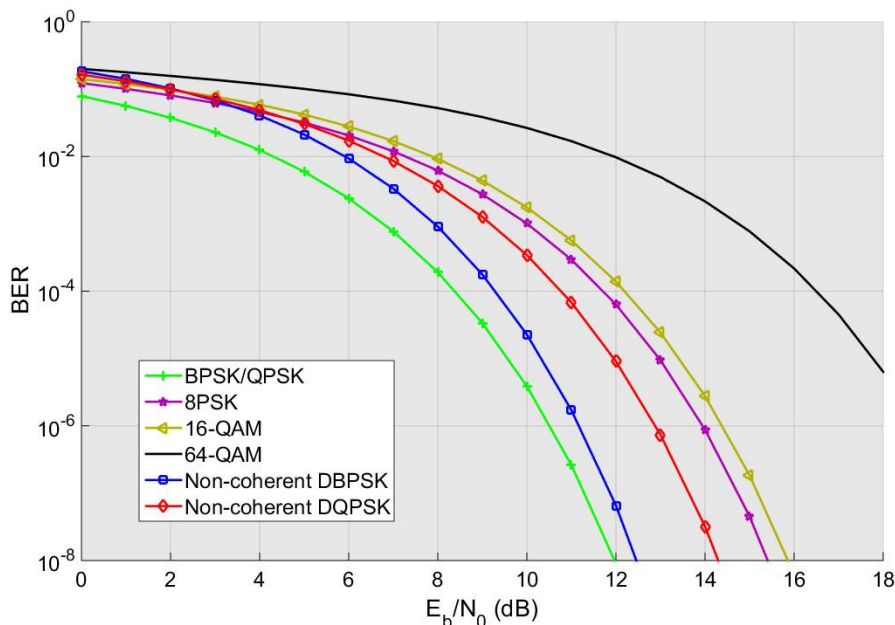


Figure 2.6: Theoretical bit error rate (BER) as a function of signal-to-noise ratio (SNR) per bit (E_b/N_0), where non-coherent DBPSK/DQPSK refers to using non-coherent detection method.

2.3 Implementation challenges in high data rate systems

A higher carrier frequency is typically required to transmit a higher data rate. Therefore, millimeter-wave bands with multiple GHz spectrum available become attractive for ultra-high capacity point-to-point links [9]. To utilize the wide channels, the associated radio systems should support wide bandwidth which is challenging for the design and implementation of the transceiver front-ends and the digital modems. The reported works presented below have addressed the challenge from different perspectives.

Owing mainly to the wide bandwidth at mm-wave spectrum, multi-gigabit transmission can be achieved using simple modulations such as binary ASK or OOK. 13 Gbps is achieved at 140-GHz band with spectral efficiency below 1 bit/s/Hz [d]. In addition, capacities up to 24 Gbps are demonstrated at 220 and 300 GHz by applying OOK [11], [13]. The main research purpose is to investigate bandwidth potential provided by recent advances in semiconductor technologies beyond 100 GHz. The applications focus on the emerging short-range communications such as imaging and sensing.

Aiming at 70/80 GHz (E-band) for future point-to-point backhaul, spectrally more efficient modulations are reported with data rate up to 10 Gbps. As limited by the sampling rate of the commercially available analog-to-digital/digital-to-analog converters (ADC/DAC), a multichannel approach based on frequency multiplexing is proposed to get around these limitations [14], [15]. A four-channel 6 Gbps system is demonstrated in 2.5 GHz bandwidth at the expense of hardware duplication at baseband and IF stage [14]. As shown in Fig. 2.7, such system requires eight FPGAs, four DACs and four ADCs to perform digital modulation and demodulation, which increases hardware cost and power consumption compared to a single channel solution.

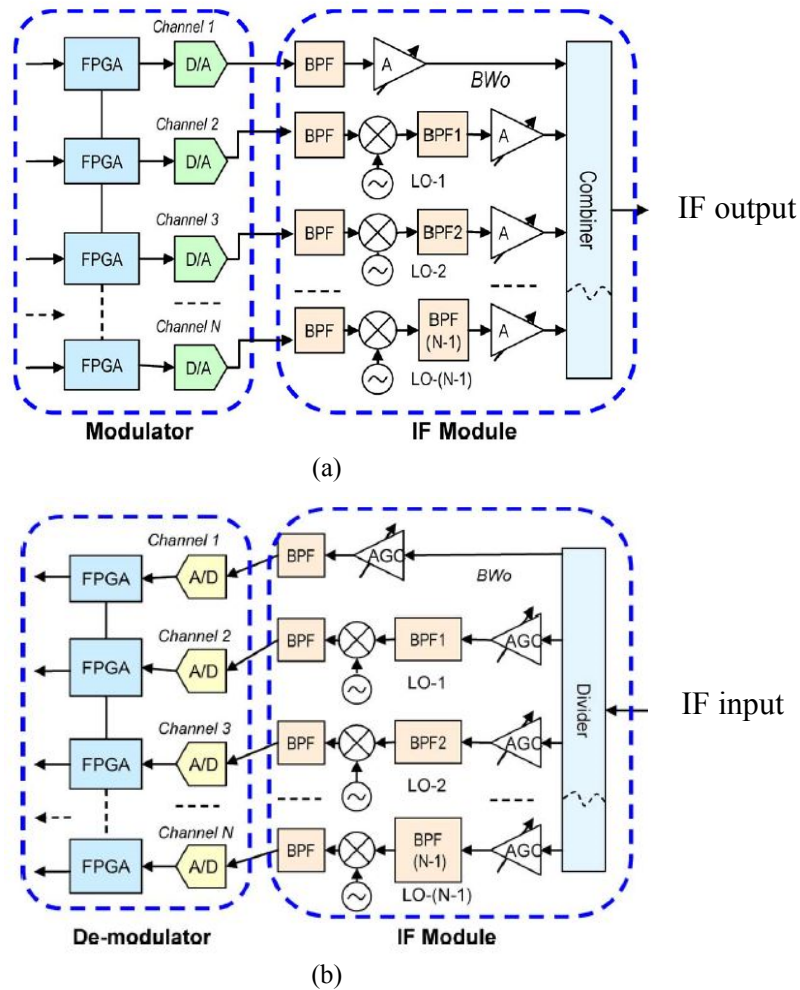


Figure. 2.7: A 6 Gbps multichannel demonstrator: function diagram of the transmitter (a) and the receiver (b) [14].

2.4 Overview of realized multi-gigabit demonstrators

In the thesis, the presented modem and system solutions demonstrate the feasibility of achieving multi-gigabit transport in a single channel with commercially available hardware at the time when the work was carried out. In Fig. 2.8, achieved data rate vs. modulation format is summarized from realized demonstrators in relevant publications.

Paper [a] presents a simple DBPSK modem (modulator and demodulator) implemented using commercially available high-speed logic gates. A GbE link at 70/80 GHz based on this modem is verified outdoor over 1 km with carrier-grade performance. The modem is attractive for systems aiming at low power consumption and low cost, requiring Gbps capacity at the expense of using wide spectrum.

The DBPSK modem scheme can be extended to DQPSK for a doubled spectral efficiency and a doubled capacity in the same bandwidth, which is demonstrated at 2.5 Gbps in paper [A]. The differential encoder as a key function is implemented in an FPGA using look-up tables (LUT). The LUTs are ROM-based so that the maximum allowed data rate depends on the FPGA memory resource. To overcome this limitation, paper [b] proposes a novel parallel prefix layer (PPL) structure for differential encoding to be data-rate scalable. A 5 Gbps

DQPSK modem is implemented and verified back-to-back with error-free performance. The 2.5 and 5 Gbps modems target point-to-point backhaul systems over E-band. Currently, such modems only operate at a fixed data rate and require hardware modification when adapted to a different rate. Paper [D] presents a data-rate adaptable DQPSK modem enabled by a new differential encoding scheme, so that mm-wave radio links based on the proposed modem can support multiple data rates without modification of the receiver. A multi-rate D-QPSK modem is implemented in a cost-and energy-efficient analog fashion, and it is tested and verified for data rates up to 10 Gbps. The data-rate limit is set by the bandwidth of the microwave components in use.

Driven by the widely used Ethernet standards, there is a demand to support 10 GbE wirelessly. Aiming at 10 Gbps over 5 GHz bandwidth in the E-band, it is necessary to apply higher order modulation, such as 16-QAM. This approach requires a digital baseband receiver with an ADC to sample the received analog signal for demodulation. A 10 Gbps test-bed is presented in paper [B], which enables 16-QAM transmission over E-band on a single carrier. Transmission performance is evaluated offline in back-to-back set-up (no free space propagation) using signal processing algorithms, specially designed for an FPGA-based digital receiver. Paper [C] describes an implementation for the digital baseband receiver which consists of an analog symbol timing recovery (STR) and a digital carrier recovery using an FPGA and ADCs. The STR is realized on “one-sample-per-symbol”, resulting in relaxed requirement on the sampling speed of the ADCs. In this sense the proposed solution is hardware efficient. A proof-of-concept E-band link is demonstrated in laboratory using the baseband receiver, which supports 5 Gbps data traffic using 16-QAM.

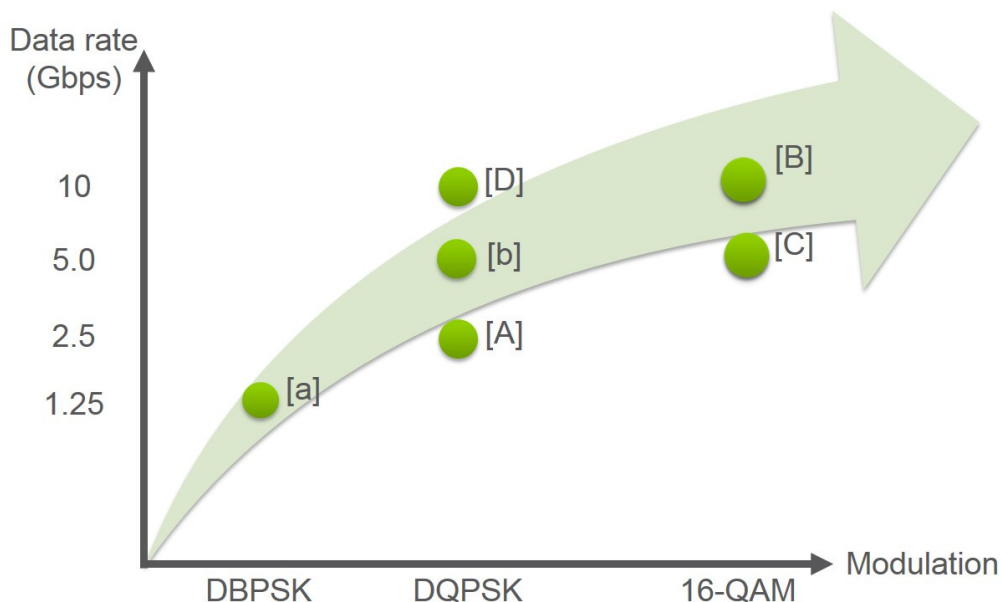


Figure 2.8: High data rate demonstrators presented in the thesis.

2.5 Challenges in wireless fronthaul networks

In future densified networks, small cells are likely to be deployed on street level at places such as lampposts, where installing fibers is not viable. High capacity and low latency wireless fronthaul links are required to support the centralized baseband architecture. Taking the advantage of wide bandwidth, it is feasible to realize multi-gigabit transmission at mm-wave frequency, as demonstrated for the backhaul. So, technology-wise, it is possible to support CPRI over wireless, the so called digital wireless fronthaul. As reported in paper [c], an E-band radio link is deployed to carry 2.5 Gbps CPRI between the baseband unit and a LTE RRU. However, the main drawback of digital fronthaul is the poor bandwidth efficiency, because the bandwidth required by the CPRI standard is much larger than the bandwidth of the actual radio signals. The data rate of the CPRI is a function of the employed radio technology and the RRU configuration. For example, the required capacity to support a single LTE RRU with 20 MHz, 3-sector, and 4x4 MIMO would be around 15 Gbps. As a consequence, digital fronthaul could limit the possibilities of capacity upgrades for future mobile networks.

2.6 Realized fronthaul demonstrators

A multi-rate DQPSK modulator/demodulator (modem) presented in paper [D] is targeted to digital fronthaul application using mm-wave. This modem is experimentally verified to fulfill the current CPRI specifications for data rates up to 10 Gbps with a BER less than 10^{-13} and a latency below 0.1 μ s. Millimeter-wave fronthaul links based on the proposed multi-rate modems provide a cost-efficient and flexible alternative to fiber optical links.

To address the drawback of the digital fronthaul, paper [F] proposes a new fronthaul concept to greatly improve the bandwidth efficiency, named analog fronthaul. The basic idea is to carry analog radio access signals over mm-wave frequency instead of multi-gigabit digital CPRI. The phase and frequency impairments introduced by high frequency carriers are effectively reduced using an analog pilot-based mitigation technique, as introduced in paper [E]. An analog fronthaul link is designed and implemented at 70/80 GHz (E-band). Thanks to the pilot-based noise mitigation, 20 MHz 64-QAM LTE uplink and downlink transmission is demonstrated over E-band with measured error vector magnitude (EVM) of about 3% at the expense of 10% pilot bandwidth overhead. The promising performance indicates that the analog fronthaul can potentially be an enabler for cost efficient and scalable fronthaul networks.

Chapter 3

Multi-Gigabit Modem and System Demonstrators

3.1 Differential QPSK modulation

Up until now, simple binary modulations, such as BPSK, have been most frequently used in high data rate systems, due to the advantages of simplicity and reliable performance. As data rate increases, a spectrally more efficient modulation is desired. For instance, QPSK doubles the data rate compared to BPSK using the same channel bandwidth, but without the performance penalty in terms of SNR. The drawback is the increased complexity of the system, because the carrier synchronization is required to perform coherent detection. Differential QPSK with non-coherent detection is a promising alternative with a relatively simple receiver at the expense of a 2.5 dB penalty of the SNR as opposed to QPSK (see Fig. 2.6).

3.1.1 Comparison of QPSK and DQPSK

In QPSK, the symbols are encoded as the phase of the carrier signal and the mapping from symbols to the phase is realized by a quadrature modulator (also known as IQ modulator). In the case of DQPSK, the symbols are encoded as the phase difference between adjacent symbols rather than the absolute phase as in QPSK. Therefore, data are recovered in the receiver by comparing the phase difference, this way avoiding the need of a synchronized carrier and results in a simple receiver implementation.

A DQPSK modulator includes a standard QPSK modulator and a differential encoder, as illustrated in Fig. 3.1. The encoder current output symbol, the k th symbol ($I(k), Q(k)$), is a function of the current input ($X(k), Y(k)$) and the preceding output ($I(k-1), Q(k-1)$). The mapping from the input ($X(k), Y(k)$) to the phase difference of the carrier is performed by the encoder, which encodes the output ($I(k), Q(k)$) as the phase difference applied to ($I(k-1), Q(k-1)$). The mapping from the encoder output ($I(k), Q(k)$) to the phase of the carrier is achieved in the same way as the QPSK modulator.

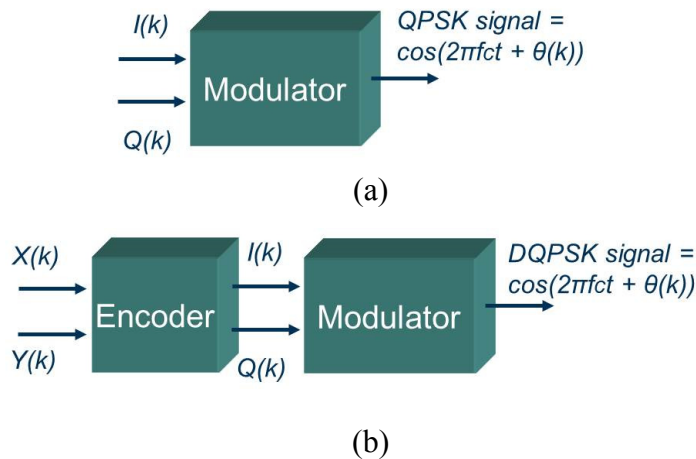


Figure 3.1: Comparison of QPSK and DQPSK, (a) QPSK modulator and (b) DQPSK modulator.

3.1.2 DQPSK modulator

A typical DQPSK modulator is depicted in Fig. 3.2. The incoming binary data are split by a Demux into two streams with odd and even bits ($X(k)$, $Y(k)$). The bits are encoded as ($I(k)$, $Q(k)$) symbols. The symbols are then modulated separately onto two intermediate frequency (IF) carriers, orthogonal to each other as generated by a local oscillator (LO) and a 90-degree hybrid. The two modulated carriers are power combined to create a DQPSK modulated signal.

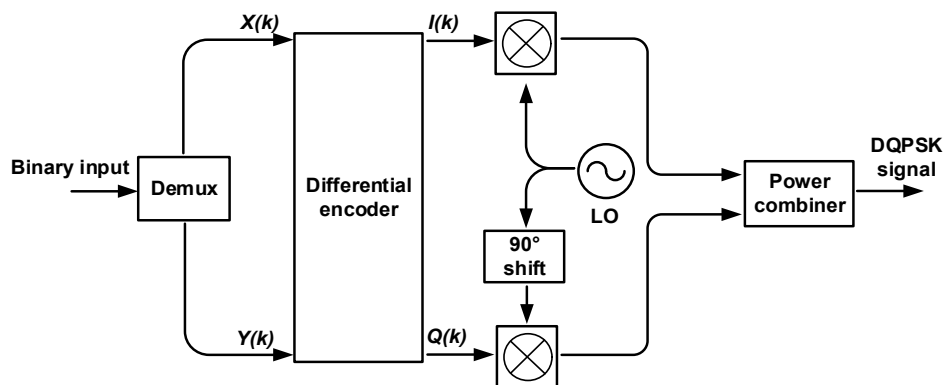


Figure 3.2: Block diagram of a DQPSK modulator.

3.1.3 Differential encoder

There are different mapping rules from ($X(k)$, $Y(k)$) to ($I(k)$, $Q(k)$) and one possible mapping is given in Table I [16]. A feedback structure is required to implement such encoders, hence named feedback encoders.

Feedback encoder

A feedback encoder can be realized using high speed logic gates, two 4-to-1 selectors and two delay-flip flops (D-FF), as shown in Fig. 3.3. It requires the outputs with one symbol delay feedback to the selector inputs, and the D-FF on each arm is served as a delay line to achieve this. The encoder works well at low data rates, as demonstrated in [17] at 200 Mbps. At

gigabit data rate, however, the propagation delay caused by the feedback routing paths is no longer negligible, and therefore, it is practically difficult to implement in discrete hardware. Instead of using D-FF devices, it may be considered to use physical delay lines to provide exactly one symbol delay. One example of a delay line on a printed circuit board (PCB) is shown in [A] for 800 ps delay corresponding to 1.25 Gbps per I/Q channel. Four such delay lines are needed in the encoder, and these have to be symmetric as they are the feedback paths. It will be very difficult to implement in a PCB design [A].

Table I: Feedback encoder mapping rule.

$X(k)$	$Y(k)$	$I(k)$	$Q(k)$	$\Delta\theta$
0	0	$\overline{I(k-1)}$	$\overline{Q(k-1)}$	π
0	1	$\overline{Q(k-1)}$	$I(k-1)$	$\pi/2$
1	0	$Q(k-1)$	$\overline{I(k-1)}$	$-\pi/2$
1	1	$I(k-1)$	$Q(k-1)$	0

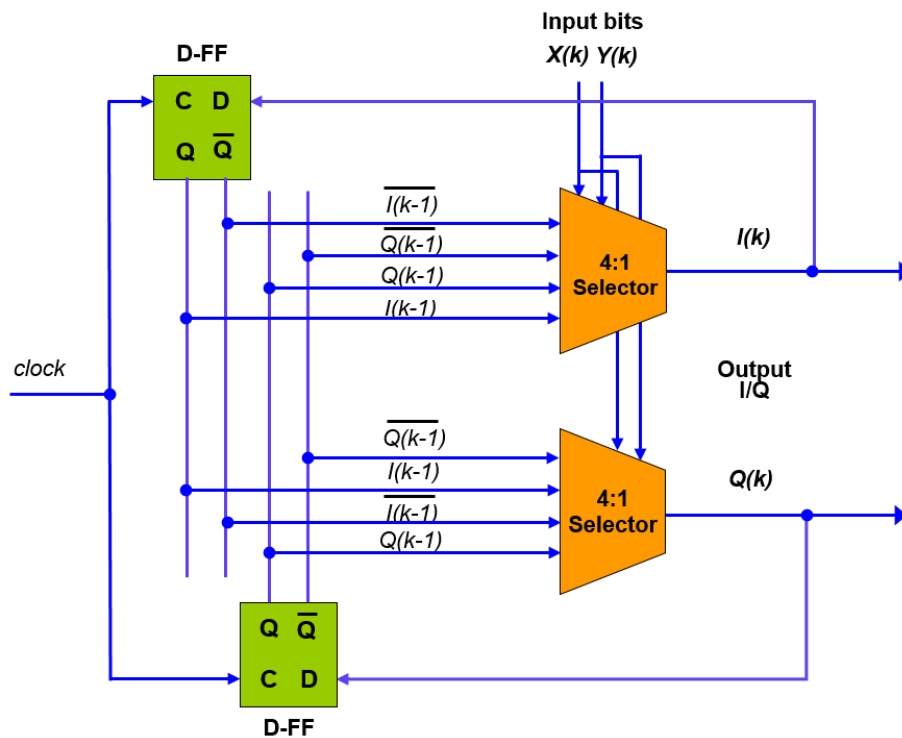


Figure 3.3: An implementation of the feedback encoder [16].

Feedforward encoder

A differential encoder without any feedback path is an alternative, the so called feedforward encoder [18]. One possible implementation is illustrated in Fig. 3.4, which consists of two exclusive-or (XOR) gates, one AND gate, two toggle-flip flops (T-FF), and one delay-flip flop (D-FF). The encoding rule is different from that of the feedback encoder, as referred to

Table I and Table II. As a result, the corresponding modulation and demodulation of the DQPSK signal is different and not as straightforward as using the feedback structure.

Table II: Feedforward encoder mapping rule.

$X(k)$	$Y(k)$	$I(k)$	$Q(k)$	$\Delta\theta$
0	0	$I(k-1)$	$Q(k-1)$	0
0	1	$I(k-1) \oplus Q(k-1)$	$\overline{Q(k-1)}$	$\pi/2$
1	0	$\overline{I(k-1) \oplus Q(k-1)}$	$\overline{Q(k-1)}$	$-\pi/2$
1	1	$\overline{I(k-1)}$	$Q(k-1)$	π

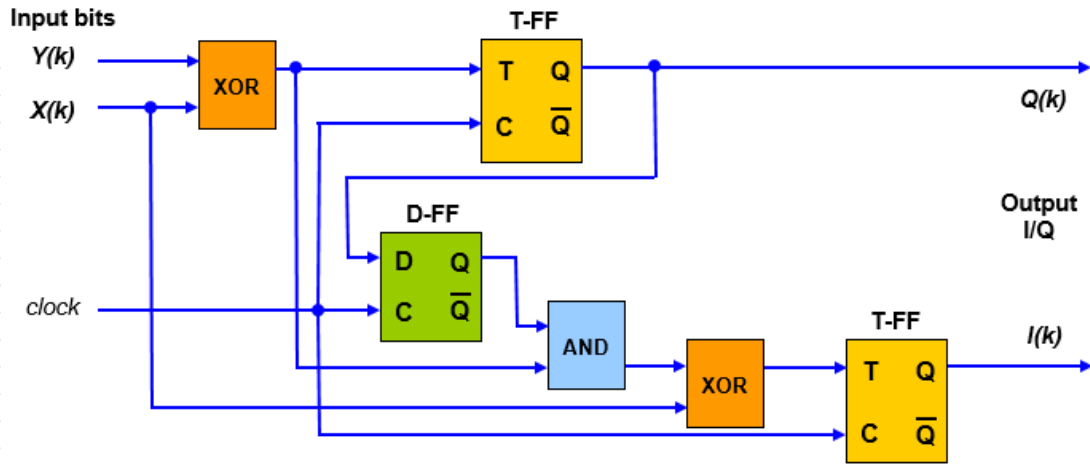


Figure 3.4: An implementation of the feedforward encoder [18].

3.2 Multi-gigabit DQPSK modems with non-coherent detection

The differential encoder is a crucial component for DQPSK modulators. High-speed encoders are not commercially available and it is a challenge to design and implement such encoders at gigabit data rate and beyond.

Feedback encoders implemented using FPGAs are demonstrated in papers [A] and [b], which enable multi-gigabit DQPSK modems aiming at point-to-point radios at E-band for mobile backhaul.

3.2.1 FPGA-based DQPSK modulator

By utilizing modern FPGAs equipped with multi-gigabit input and output ports, it is possible to realize high data rate FPGA-based modulators. In paper [A], a differential encoder working up to 2.5 Gbps, shown in Fig. 3.5, is implemented in an FPGA based on the encoding rule in Table I. Inspired by the symmetric encoding rule, two ROMs (read-only memory) are used to perform the encoding operation with a 2-bit memory to store the last IQ symbol. The correct ROM output is selected by the state of the last symbol. To accommodate the low clock speed in the FPGA, a high speed serial data at 2.5 Gbps is split into 16-bit-width data so that the

logic operation is at 156.25 MHz [A]. A DQPSK modem using this encoder is experimentally verified with error-free transmission.

A drawback of the ROM-based encoder is that the maximum data rate is limited by the memory currently available in FPGAs. Since the number of parallel bits (bit-width) increases at higher data rates, the memory usage is especially high. To overcome this limitation, a data-rate scalable encoding algorithm using a parallel prefix layer (PPL) structure is proposed in paper [b]. Based on the parallel prefix network (PPN) in [19], the PPL algorithm is developed to increase the speed of operation and reduce the need of hardware resources. A 5 Gbps encoder is demonstrated in the same FPGA platform as in [A], which would have been impossible to implement if the ROM-based encoding was used.

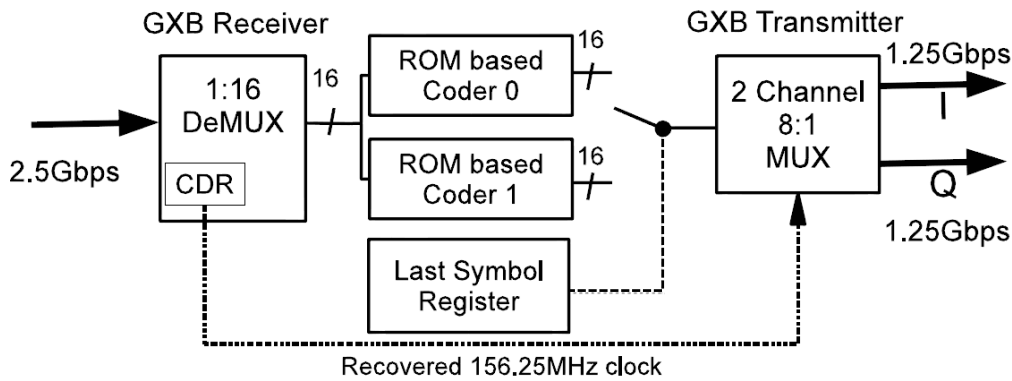


Figure 3.5: FPGA-based differential encoder [A].

3.2.2 DQPSK demodulator implementation

In a DQPSK demodulator, the symbols are recovered by comparing the phase difference between the current symbol and the preceding symbol of the received signal. The demodulator in Fig. 3.6 (a) is a straightforward implementation of the given encoding rule (Table I), which requires $\pm 45^\circ$ phase shift to define the decision lines of the DQPSK constellation. With considerable design efforts, such a demodulator is implemented at 2.5 Gbps in paper [A] using two voltage-controlled phase shifters, 90° out of phase, and two identical symbol-delay elements.

Theoretically, the structure would work for higher data rates if the low pass filters (LPF) and the symbol-delay paths were updated accordingly. However, the hardware implementation is critical considering the high accuracy required for the phase and delay tuning. An improved demodulator structure is proposed in paper [b], suitable for high data rate applications. As shown in Fig. 3.6 (b), it is functionally equivalent to the old structure, but the number of the tuning parameters is reduced from four to one, and it is thus more robust against delay/phase misalignment. The symbol delay is implemented together with the 45-degree phase shift by a tuneable delay element, which is the only adjustable parameter. The delay is tuned to provide a time delay of one symbol period plus a 45-degree phase shift at the IF carrier frequency.

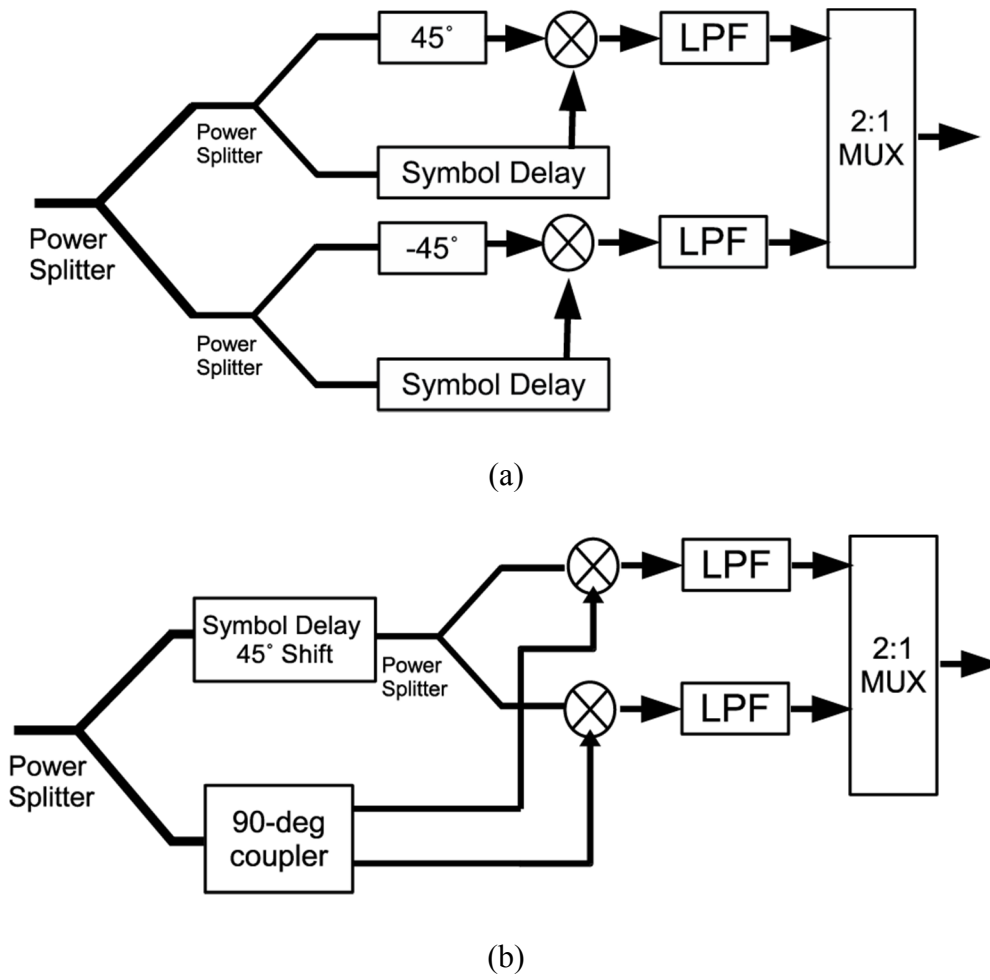


Figure 3.6: Possible implementations of a DQPSK demodulator, (a) the 2.5 Gbps demodulator in paper [A] and (b) the 5 Gbps demodulator in paper [b].

3.2.3 Multi-rate DQPSK modem implementation

The presented DQPSK modems in paper [A] and [b] are designed for a fixed data rate. The FPGA-based differential encoder is data-rate scalable through software upgrade of the FPGA [b]. However, it is not possible to adjust the decoder/demodulator to different data rates without hardware change, because the symbol-delay element is implemented using a fixed-length transmission line.

Paper [D] introduces a novel differential encoding scheme, which enables data-rate adaptable DQPSK transmission without any hardware modification of the receiver. A multi-rate DQPSK modem is implemented using the same hardware platform as in [b]. The performance of the modem is verified at data rates up to 10 Gbps. The data rate is limited by the bandwidth of the microwave components in use.

Proposed multi-rate differential encoding

In conventional differential encoding, the current symbol $s_{i+1}(t)$ is encoded as a phase difference $\Delta\varphi_i$ applied to the previous symbol $s_i(t)$, as shown in Fig. 3.7 (a). To perform differential detection, a time delay of exactly a symbol period T_s is needed. When the data rate is doubled, the symbol period is reduced from T_s to $T_s/2$, as shown in Fig. 3.7 (b). As a

consequence, the provided time delay should be reduced to half as well, which is hardware-wise not straightforward to implement, as discussed in [D].

A new differential encoding scheme is presented for multi-rate detection using a constant time delay element. The proposed differential encoding rule is shown in Table III, where N is the multi-rate factor. When $N=1$, the base rate, the proposed scheme is identical to the conventional scheme. The basic idea of the proposed scheme is the following: when the data rate is N times the base rate, data are encoded by applying a phase difference of $\Delta\varphi_i$ between i^{th} symbol and $(i+N)^{\text{th}}$ symbol (the N^{th} nearest neighboring symbol), instead of applying $\Delta\varphi_i$ between two adjacent symbols.

An example is given in Fig. 3.7 (c) to illustrate the idea, when the data rate is doubled ($N=2$). In this case, the required time delay is two symbol periods, $2 * T_s/2$. Since the symbol period for $N=2$ is half of that for the base rate $N=1$, the required time delay becomes actually the same as that for the base rate. Similarly, the proposed encoding scheme can be scaled up to higher data rates. As explained in Fig. 3.7 (d), when the data rate is tripled ($N=3$), the identical amount of time delay as for the base rate $N=1$ in Fig. 3.7 (a) should be used in the receiver.

Therefore, a DQPSK modem based on the new encoding could operate at multiple data rates without changing the physical delay in the receiver. However, one limitation with the new encoding is that it is not applicable to an arbitrary data rate. The data rate must be an integer multiple of a base rate.

Table III: Proposed differential encoding rule [D].

B_0	B_1	I_{i+N}	Q_{i+N}	$\Delta\varphi_i$
1	0	\overline{Q}_i	I_i	270°
0	0	\overline{I}_i	\overline{Q}_i	180°
0	1	Q_i	\overline{I}_i	90°
1	1	I_i	Q_i	0°

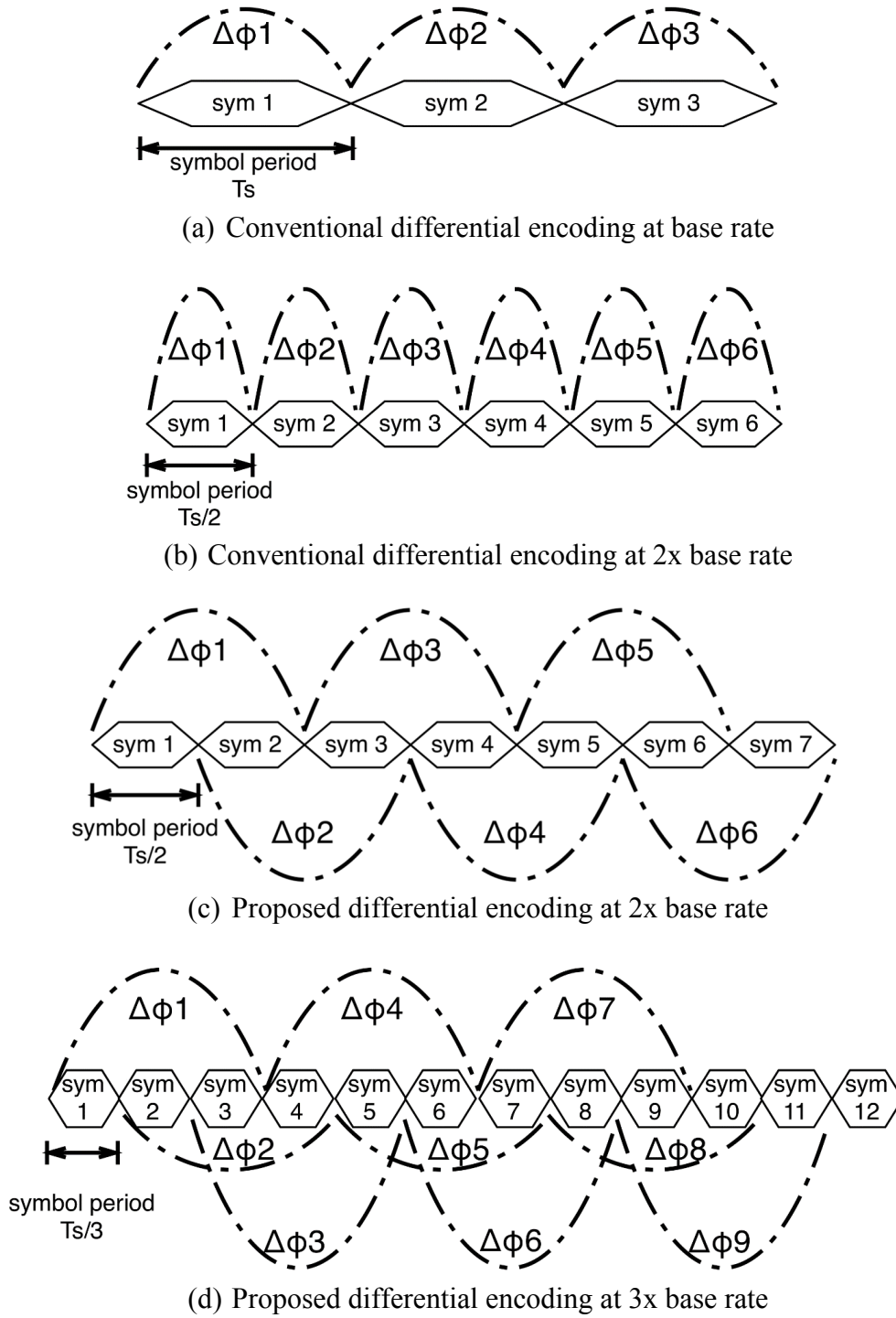


Figure 3.7: Comparison of proposed differential encoding and conventional encoding, where T_s is the symbol period [D].

Multi-rate modem measurement

The modem is tested for BER in an IF back-to-back set-up. Such a measurement is performed at 2.5, 5 and 10 Gbps, and the modem achieves error-free transmission (assume BER of 10^{-13} as the receiver threshold) at all rates for different PRBS lengths (from PRBS-7 to PRBS-13). With the possibility to adjust the signal power to the demodulator, BER is measured as a function of the demodulator input power, as presented in Fig. 3.8. The demodulator dynamic range shrinks as the data rate increases, which is attributed to the increased noise power at a higher data rate (wider bandwidth) that reduces the SNR. Nonlinear impact of the demodulator is shown at high input power, which can be improved with an automatic gain control function. In addition, the performance of the proposed DQPSK encoding is compared with the conventional encoding and the measurement results show identical performance.

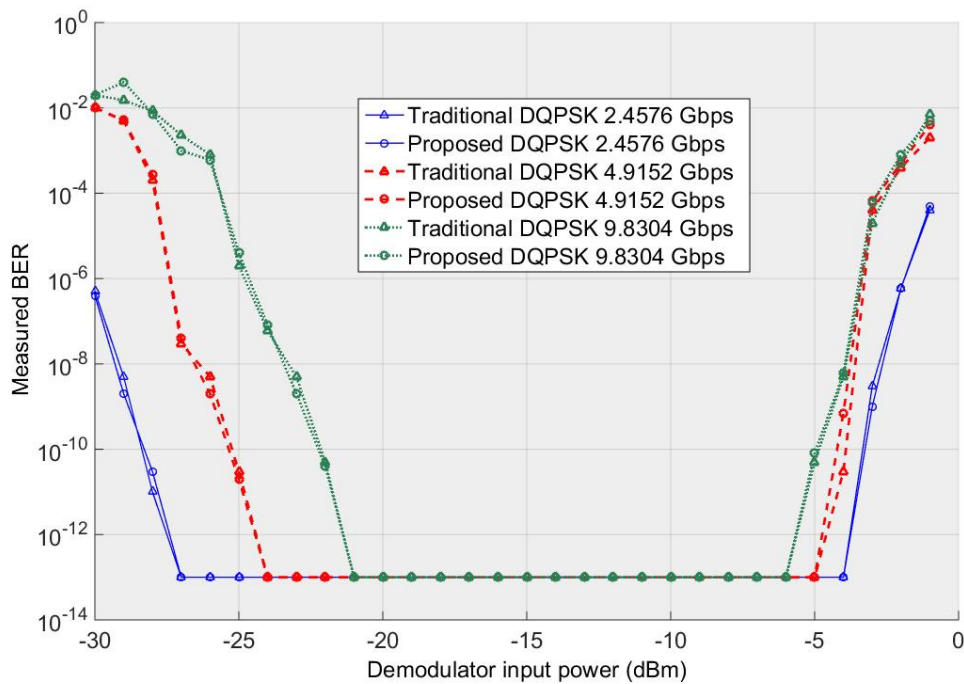


Figure 3.8: Performance comparison between the proposed differential encoding and conventional encoding at different data rates.

3.3 Spectrally efficient modems with coherent detection

Multi-gigabit transmission in mm-wave bands has been demonstrated using relatively simple modulations, such as DBPSK and DQPSK. However, to further increase the data rate, applying a high order modulation is an efficient tool. Aiming to 10 Gbps over 70/80 GHz (E-band), 16-QAM modulation is necessary to use for the given 5 GHz bandwidth. A 16-QAM based system requires the receiver to perform coherent detection, where a digital receiver is often used with an ADC to sample the received analog signal for digital signal processing. According to the Nyquist sampling theorem, the sampling rate shall be higher than the Nyquist rate, which is twice the symbol rate in the context of a bandwidth limited baseband signal.

3.3.1 Synchronization in coherent detection

In coherent detection/demodulation, the reference signal at the receiver must be synchronized with the received signal in frequency and phase. Receiver synchronization includes carrier synchronization and symbol synchronization. Carrier synchronization can be achieved by carrier recovery (CR) to remove frequency and phase differences between the carrier of the received signal and the receiver local oscillator. Symbol synchronization is achieved by symbol timing recovery (STR) to obtain the optimum sampling point with the best SNR.

Fig. 3.9 displays a 16-QAM constellation before and after synchronization. Three circles with difference in amplitude start to be visible after the STR, which show the impact of a carrier offset. Once the CR is performed, the rotating effect is removed so that a decision can be made in the slicer by quantizing the symbols to the nearest constellation points.

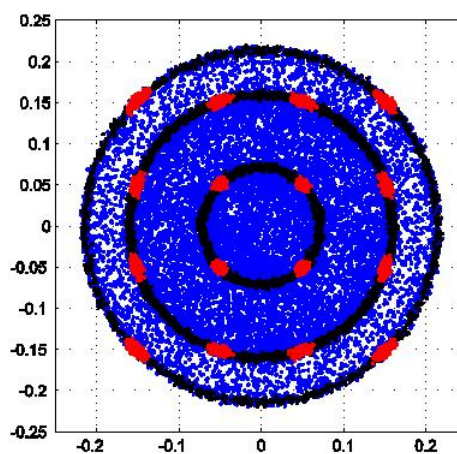


Figure 3.9: 16-QAM constellation plot showing received data before STR (in blue colour), after STR (in black) and after CR (in red).

Symbol timing recovery

Symbol timing at the receiver must be synchronized with the received signal in frequency and phase. Hence, both the sampling frequency and the sampling phase shall be recovered to ensure that the samples are taken at a correct rate and sampling is taken place in the middle of the symbol period to give the best SNR.

There are two types of STR: open-loop synchronization (feedforward STR) and closed-loop synchronization (feedback STR) [20]. The open-loop synchronization recovers the clock from the demodulated data stream by non-linear operations on the received signal. In this case the STR is performed in the analog domain and is independent of the ADC to relax the requirement on the sampling rate. The closed-loop synchronization uses the demodulated data stream to control a clock signal generated from a local oscillator by comparative measurements. The classic early-late gate algorithm [20] is a closed-loop example, where the sign of the error signal determines if the sampling occurs too late or early. In the digital domain, the generation of the error requires ADC oversampling, at least three samples per symbol. It is thus not practical for high data rate systems.

Carrier recovery

Any frequency or phase offset causes the received signal constellation to rotate. In order to correctly detect the symbols, the receiver must provide accurate carrier frequency and phase estimates by carrier recovery. The carrier recovery is performed in two steps, where carrier frequency offset shall be compensated before the phase offset compensation.

Carrier recovery for QAM modulations can be achieved in two ways [20]. One is the well-known fourth-power loop. It produces a spectral line at $4*fc$, which is locked by a PLL and is then divided by four to generate a wanted carrier at frequency fc with the same phase as the received signal. Another is the decision-directed carrier recovery (DDCR). In the DDCR technique, the receiver demodulates the current symbol and makes a decision as to which it thinks is the most likely corresponding transmitted symbol in the constellation. The phase difference between the received symbol and the constellation point is the feedback error to update the carrier recovery process accordingly.

3.3.2 Overview of published spectrally efficient solutions

Modern communication systems employing high order modulations often use a digital baseband receiver equipped with ADCs. The implementation of STR often requires the ADC to operate at a sampling rate several times higher than the receiver bandwidth (or symbol rate), the so-called oversampling. This implies that the sampling rate of the ADCs may well be a bottleneck limiting the maximum achievable data rate of the systems. A 10 Gbps 16-QAM system is described in [21], which requires 4x sampling rate relative to the symbol rate because of the timing synchronization algorithms. However, limited by the sampling rate of the commercially available ADC/DAC, a hardware-based demodulator is implemented operating at 2 Gbps. To overcome the barrier, a solution commonly used is to apply multiple parallel channels and have a digital receiver with a low sampling rate ADC for each channel. For example, a 6 Gbps 8-PSK is demonstrated using four channels to afford a sampling rate at 3x the symbol rate in [14]. Similarly, eight channels are used to construct a 10 Gbps 16-QAM system in [15]. It is obvious that multi-channel solution requires more hardware and consumes more power compared to a single channel solution.

In paper [C], a hardware-efficient baseband receiver is proposed. The basic idea is to realize STR based on only one sample per symbol, which relaxes the requirement on the ADC sampling rate. In this sense the proposed solution is hardware efficient. In reality it can be beneficial for two reasons: 1) For a given sampling rate, the ADC is applicable to a higher symbol rate as compared to using oversampling. 2) For a given symbol rate, it is possible to use lower-end ADCs to decrease cost and power consumption.

3.3.3 Implementation of a hardware-efficient 16-QAM demodulator

A proof-of-concept baseband receiver is implemented based on a dual channel ADC at a sampling rate of 1.25 GSps (gigasample per second). As an example, 16-QAM is chosen as the modulation format and the baseband receiver is able to demodulate at 5 Gbps, which is 1.3 time higher than the maximum data rate allowed by the ADC if the lowest sampling factor reported so far would have been used in the implementation [22].

The proposed baseband receiver, depicted in Fig. 3.10, consists mainly of an analog STR block and a digital CR block. The received IF signal is down converted to baseband I and Q signals. The symbol clock is recovered in the analog domain by non-linear operations on the received IF signal, the open-loop synchronization approach. Driven by the received symbol clock, a dual-channel ADC takes one sample for each symbol and the sampled data are real-time processed in an FPGA for carrier synchronization.

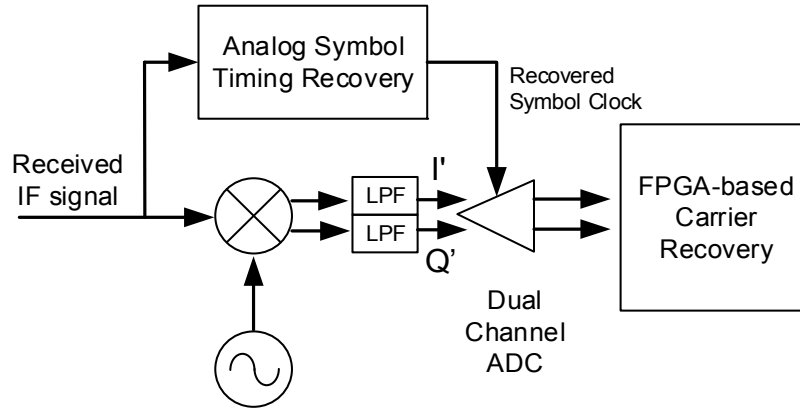


Figure 3.10: Proposed baseband receiver [C].

Analog symbol timing recovery

Fig. 3.11 (a) presents the block diagram of the proposed STR. The clock frequency is generated through the delay-and-multiply operation on the received analog signal. The length difference of two transmission lines TL_1 and TL_2 provides a true time delay of one symbol period. The TL_1 and TL_2 can be implemented as 50-Ohm micro-strip lines with the possibility to adjust the length of TL_2 using 0-Ohm resistors R_0 , as shown in Fig. 3.11 (b). The time delay could be adjusted by approximately ± 5 ps using this approach. A pronounced frequency component at the symbol clock rate (1.25 GHz) after the LPF is clearly observed in simulation (Fig. 3.11 (c)). To extract the symbol clock, a commercial clock and data recovery (CDR) module (Silicon Lab, Si5023) is used instead of a classic band pass filter, which contains a limiting amplifier and a digital phase-locked loop (DPLL). The recovered symbol clock is generated by the PLL that is locked to the symbol rate frequency component. The PLL frequency is set to be 1.2488 GHz with 120 MHz bandwidth, which covers the frequency range of interest with sufficient margin. To ensure samples are taken by the ADC at the center of each symbol period, the sampling phase needs to be aligned. The sampling phase alignment is implemented using an FPGA, which controls the ADC internal programmable clock delay to maximize the amplitude of acquired I and Q samples. It is sufficient to adjust the ADC clock delay over one symbol period (800 ps).

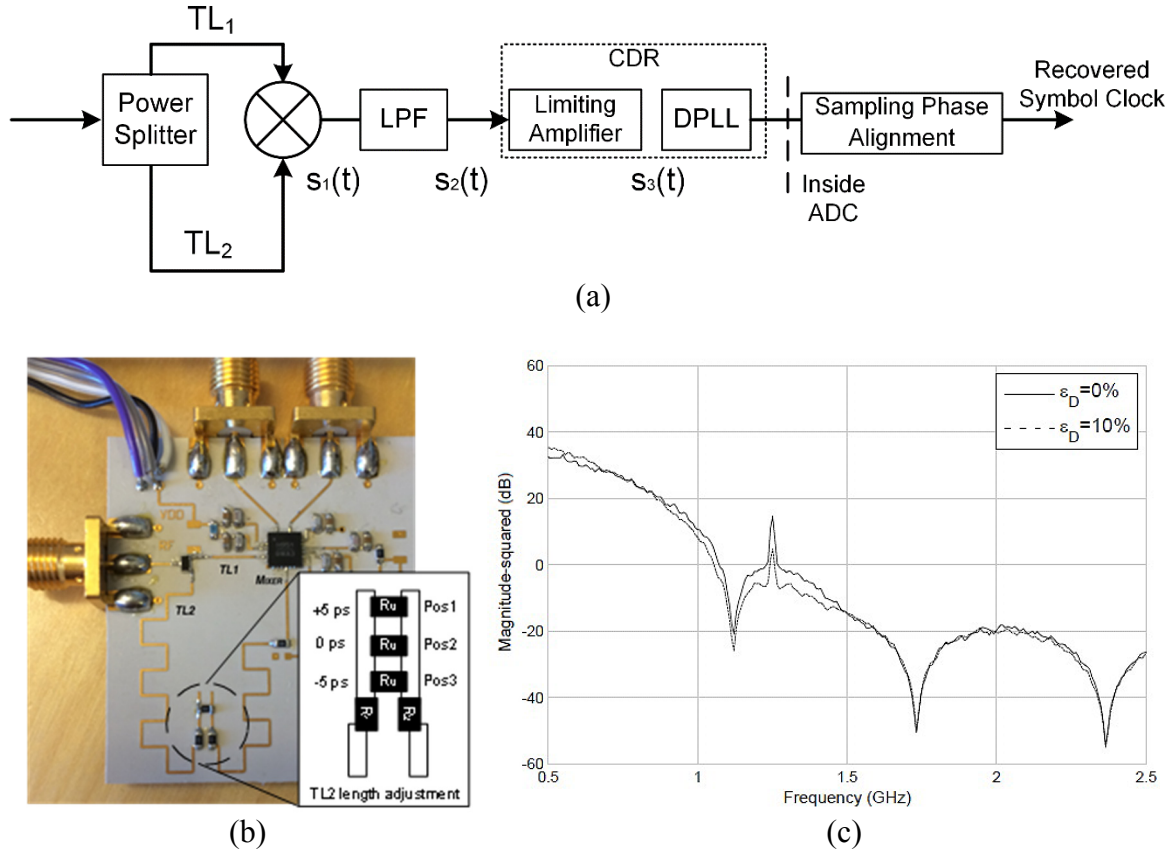


Figure 3.11: Proposed analog symbol timing recovery (STR), (a) block diagram of the STR (b) implementation of delay lines (TL_1 and TL_2) on PCB, and (c) simulated spectrum of $S_2(f)$ after LPF [C].

FPGA-based carrier recovery

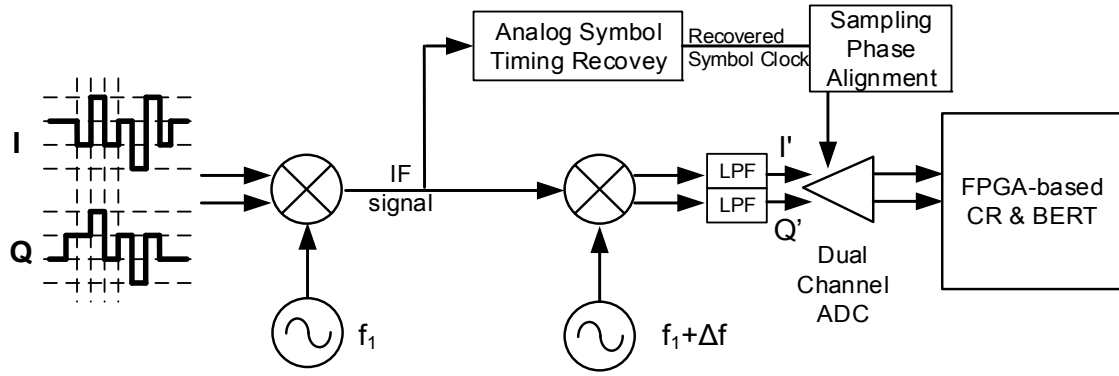
The carrier recovery (CR) is implemented in an FPGA using a parallel processing structure so that the FPGA clock speed is reduced to be one quarter of the symbol rate. The algorithm is based on decision-directed CR technique, and detailed structure is presented in paper [C]. With a practical implementation in mind, the algorithm is designed to reduce the amount of FPGA hardware resources used, such as the multiplier resolution and the number of multipliers. As a result, a digital design including the CR, a BER tester and a logic analyser function can be realized using the smallest FPGA device (XC4VSX25) in Xilinx Virtex-4 family.

Baseband receiver measurement

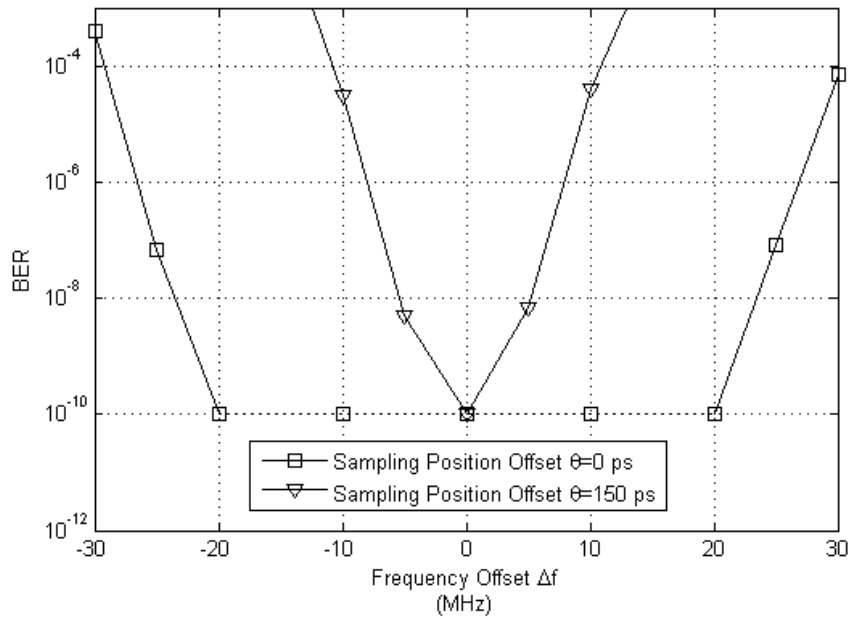
The function of the baseband receiver is verified in an IF back-to-back set-up as illustrated in Fig. 3.12 (a), where the analog STR is tested together with the FPGA-based CR. An arbitrary waveform generator (AWG) is used to provide the multi-level 16-QAM I and Q symbols from a PRBS-9 data sequence. A frequency offset Δf is inserted between the transmitter and the receiver LOs. The Δf is varied to investigate the CR operational frequency range. The ADC sampling clock is recovered from the analog STR and the sampling phase alignment is turned on and off to study the impact of the sampling phase offset on the CR performance. The BER

tester (BERT) implemented in the FPGA is capable to calculate the error rate down to 10^{-10} , which is the limit defined by the FPGA hardware resources.

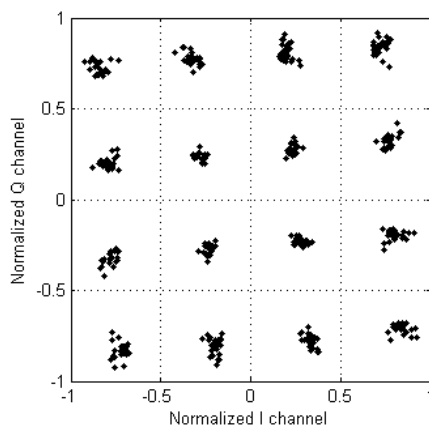
Fig. 3.12 (b) shows the measured BER as a function of the frequency offset. When the sampling phase is perfectly aligned (sampling phase offset = 0), error-free transmission is achieved in the measurement ($BER \leq 10^{-10}$) with +/-20 MHz frequency offset. In the presence of a 150 ps sampling phase error, the CR range is reduced to +/-5 MHz ($BER \leq 10^{-8}$). A frequency stability of +/-10 ppm is a typical performance of commercial oscillators, which means +/-3.44 MHz offset at 86 GHz carrier frequency. Therefore, the frequency range of the CR is not a concern for the E-band application. As an example, Fig. 3.12 (c) displays the constellation diagram after CR when the frequency offset is 0.5 MHz with sampling phase alignment enabled.



(a)



(b)



(c)

Figure 3.12: Receiver measurement, (a) block diagram of the test set-up, (b) measured BER as a function of frequency offset applied between the transmitter and the receiver, and (c) measured constellation after CR (16384 samples) [C].

3.4 Multi-gigabit systems

10 Gbps and beyond will be required for wireless backhaul in future networks. It is technically feasible to support 10 Gbps wirelessly, see the reported works summarized in Table IV. Owing mainly to the wide bandwidth used in 120 GHz band, 10 Gbps transmission is achieved by using simple modulations, such as OOK and QPSK [23], [24]. When applying a spectrally more efficient modulation, a 10 Gbps radio link at 70/80 GHz is reported using eight channels in [15]. However, the hardware cost and power consumption are the main concerns in practical applications. A single-channel 10 Gbps system over 140-GHz band is described in [21]. Due to the limitation of the ADC sampling rate, a real-time demodulator is implemented operating at 2 Gbps instead of 10 Gbps.

Table IV: Summary of reported 10 Gbps system demonstrators.

Frequency band	Modulation	Data rate (Gbps)	Detection method	Ref
120 GHz	ASK/OOK	10	Envelop detection	[23]
120 GHz	QPSK	10	Differential detection	[24]
140 GHz	16-QAM	10	Offline detection	[21]
		2	Coherent detection	[21]
70/80 GHz	16-QAM	10	8-channel Coherent detection	[15]
70/80 GHz	16-QAM	10	Offline detection	[B]
		5	Coherent detection	[C]

3.4.1 5/10 Gbps system demonstrators at 70/80 GHz (E-band)

Paper [B] presents the implementation of a single-carrier 10 Gbps radio test-bed at 70/80 GHz and digital receiver algorithms to mitigate hardware impairments for the given system specifications. In addition, the algorithms are designed to minimize computation complexity, applicable for an FPGA-based receiver implementation. The radio link performance is evaluated for 10 Gbps 16-QAM transmission in a loop-back set-up. The received signal is demodulated offline to characterize the hardware channel and to validate the developed receiver algorithms.

The research effort in paper [B] is in preparation for real-time transmission and detection of 10 Gbps over 70/80 GHz. However, to accommodate the sampling rate of the ADC on a currently available FPGA platform, a 5 Gbps 16-QAM baseband receiver is implemented and verified [C]. Moreover, a 5 Gbps E-band link based on the receiver is constructed and tested in lab, as shown in Fig. 3.13. The 16-QAM baseband I and Q symbols are generated from an arbitrary waveform generator (AWG). The E-band transmitter and the receiver are connected using waveguides and a variable attenuator so that the input power to the E-band receiver could be adjusted. Timing and carrier synchronizations are performed using the proposed receiver, which also calculates BER. The E-band link performance is characterized with BER

measured as a function of the received input power. Measurement results in Fig. 3.14 show error-free transmission ($BER \leq 10^{-10}$) achieved when the input power is higher than -47 dBm.

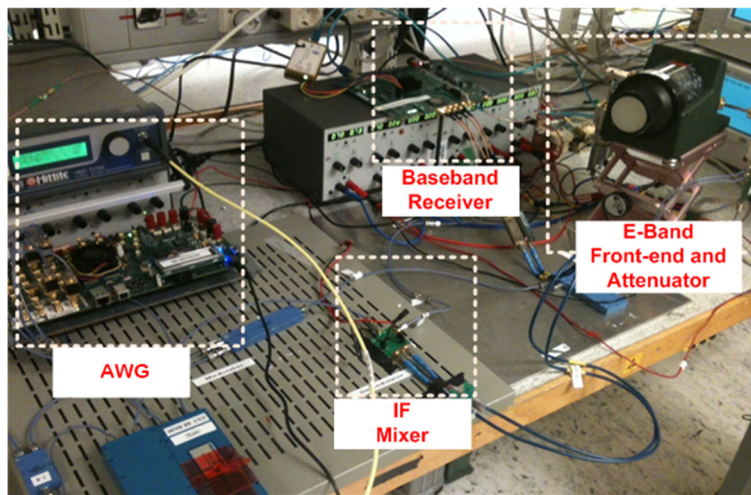
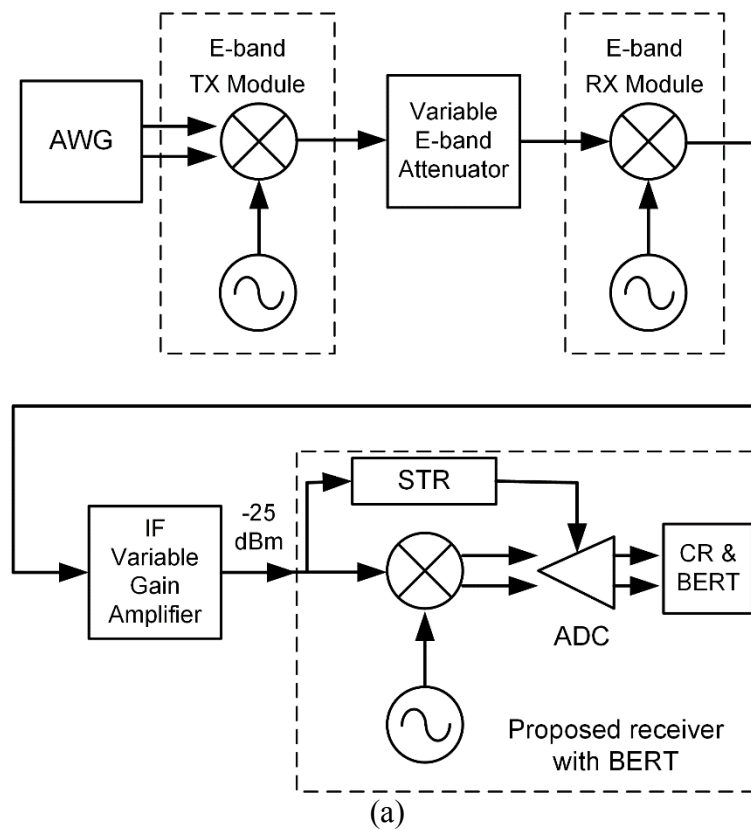


Figure 3.13: System measurement set-up, (a) block diagram and (b) photo of the experimental set-up in the laboratory [C].

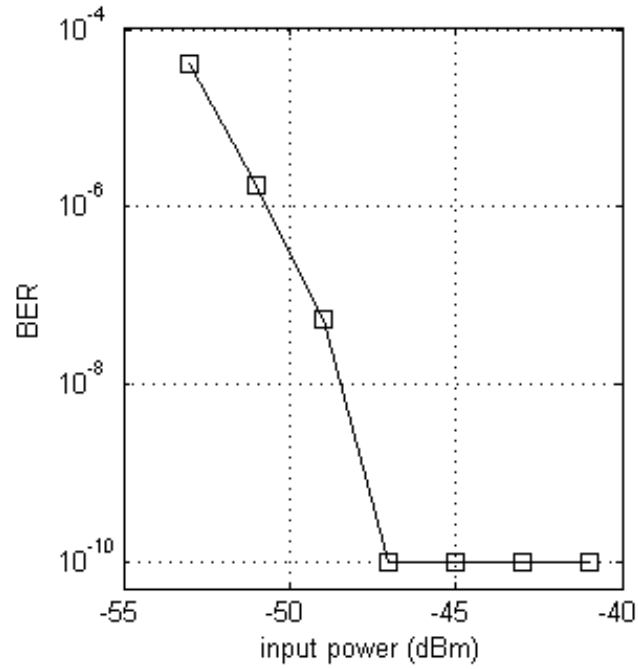


Figure 3.14: Measured BER over 70/80 GHz (E-band) as a function of input power to the E-band receiver [C].

Chapter 4

Millimeter-wave Fronthaul Demonstrators

4.1 Digital fronthaul

Digital fronthaul links carry digital CPRI information between the BBU and the RRU. As depicted in Fig. 4.1 (a), digital fronthaul is typically fiber-based using digital radio over fiber (D-RoF) technology, while it is also possible to realize CPRI transmission over wireless, see Fig. 4.1 (b). The CPRI standard specifies data rate at an integer (n) times a base rate 614.4 Mbps, where $n = 1, 2, 4, 5, 8, 10, 16$ when using 8B/10B line coding, and the highest rate is 9.8304 Gbps [6]. High capacity wireless links are thus required to support digital fronthaul. Millimeter-wave technology, thanks to the available wide bandwidth, is the most promising choice to realize wireless transmission of multi-gigabit CPRI. For example, Ericsson demonstrated the world's first CPRI transmission over a 2.5 Gbps E-band radio link between a LTE BBU and a RRU [c].

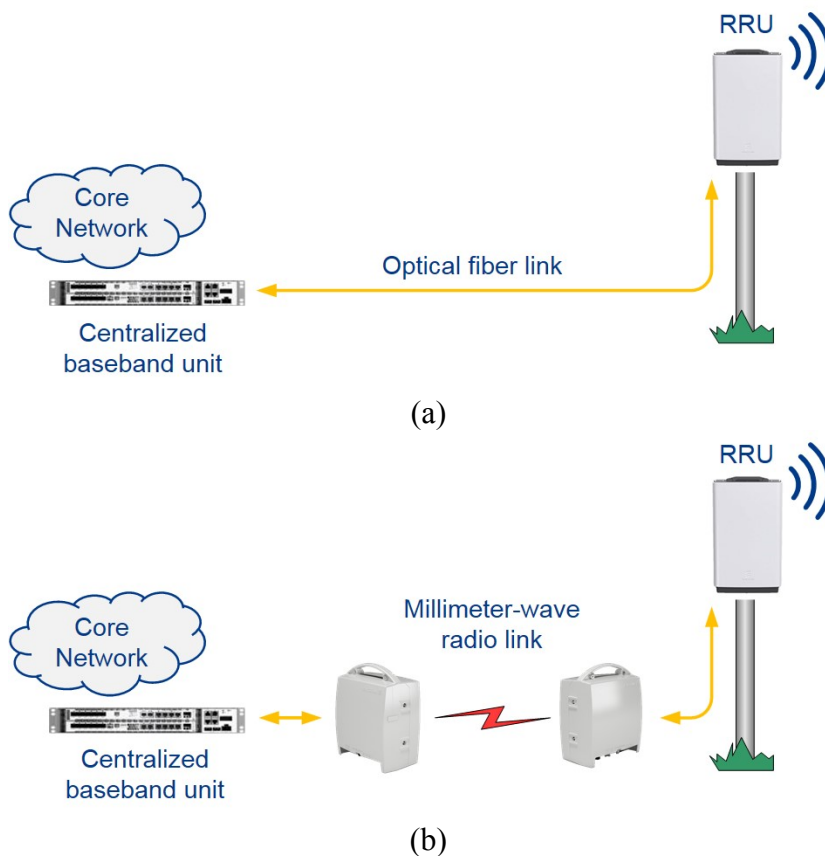


Figure 4.1: Digital fronthaul link technologies, (a) fiber-based fronthaul and (b) wireless fronthaul.

4.1.1 Fixed-rate demonstrator

The 70/80 GHz band (E-band) with a total bandwidth of 10 GHz allows multi-gigabit transmission using relatively simple modulation schemes. The demonstrated E-band radio link is an all-outdoor unit based on DBPSK modulation and equipped with a 2.5 Gbps optical interface, as shown in Fig. 4.2. The modulator and demodulator are implemented using commercially available high speed exclusive-or (XOR) gates [a]. This implementation decreases power consumption by avoiding using digital processing devices and mixed signal devices. Thereby it also reduces the cost. The simple implementation leads to a low power consumption, a low cost and a very low latency wireless solution for high data rate transmission.

A digital wireless fronthaul link was demonstrated for the first time in an LTE trial in December, 2011, where 2.5 Gbps CPRI data was carried over the E-band radio link using full duplex transmission [c]. As illustrated in Fig. 4.3, the baseband unit inside the building (main site) was connected via fiber to one E-band radio mounted on the roof top, while the remote radio unit was placed about 200 meters away on top of a truck (remote site) and fiber connected to another E-band radio. The main-remote connection was established over the E-band link, and a user terminal download speed of 60 Mbps was demonstrated with the RRU configured as a small cell. Wireless fronthaul solutions offer great flexibility for operators to deploy remote radios where most needed, which is considered to be crucial for small cell deployment in heterogeneous networks [c].

Similar to the 2.5 Gbps demonstrator, radio links based on the realized DQPSK modems at 2.5 Gbps and 5 Gbps are also possible to use for CPRI transmission. In fact, due to analog implementation of the modems the radios are protocol transparent with no restriction on what data or service they carry, which is desirable in networks with a mixture of CPRI and Ethernet links for both fronthaul and backhaul applications.

However, the radios can only support a fixed data rate, like the multi-Gbps wireless links reported in relevant studies such as [a], [A], [b]. It is not possible to adapt such radio systems to different data rates without hardware changes. It is a drawback in the fronthaul application not to be able to support the full range of CPRI rates.

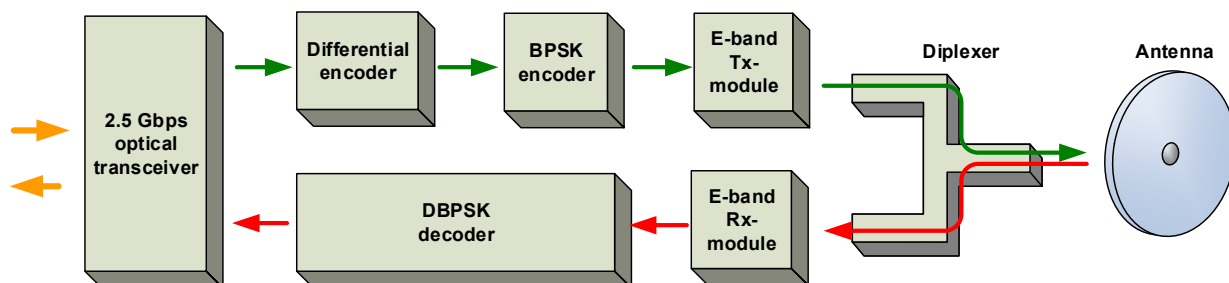


Figure 4.2: Block diagram of the 70/80 GHz radio demonstrator [a].

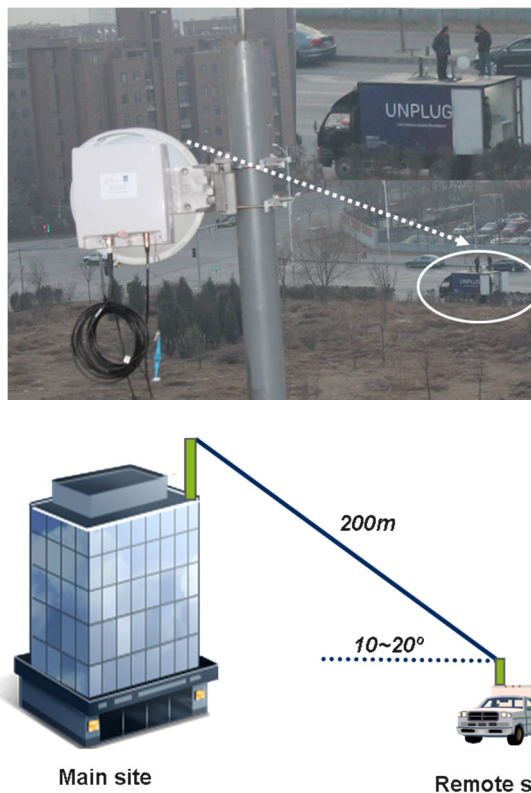


Figure 4.3: Demonstration of CPRI over E-band link, Beijing, 19th December 2011 [c].

4.1.2 Adaptable data-rate demonstrator

In paper [D], we propose a data-rate adaptable DQPSK modem solution for digital wireless fronthaul links at mm-wave bands. The modem is based on a novel differential encoding scheme so that it supports multi-rate operation without any hardware modification of the receiver. The modem data rate must be an integer multiple of a base rate, which is well suited for a full range of CPRI rates, at integers time the base rate 614.4 Mbps.

A DQPSK modem is constructed using commercial components and tested for data rates up to 10 Gbps, this being the limit given by the bandwidth of the microwave components in use. The modem is verified and fulfils the CPRI specifications with respect to multi-rate, low latency and high system performance. The detailed modem implementation and measurement results are presented in [D].

Based on this modem, an E-band radio link is demonstrated at 5 Gbps in laboratory environment for proof-of-concept. As the set-up shown in Fig. 4.4, the two radios are connected through a waveguide interface with added attenuation but without antennas. Due to the bandwidth limitation of the E-band transceivers, the maximum data rate of such a link is 5 Gbps for DQPSK modulation in a duplex scheme. The link performance is measured and error-free transmission ($BER < 10^{-13}$) using PRBS-13 data sequence is achieved when 30 dB attenuation is applied between the transmitting and the receiving radios.

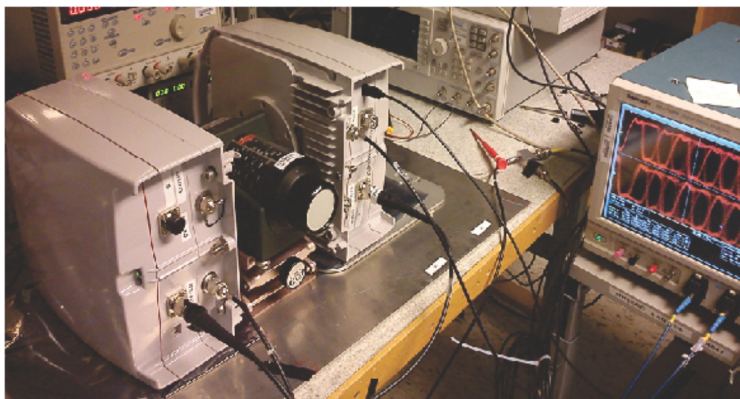


Figure. 4.4: Laboratory test-bench of an E-band radio link using the proposed multi-rate modem [D].

4.2 Analog fronthaul

The feasibility of digital wireless fronthaul has been demonstrated as described in the previous section. The demanding CPRI transmission requires bandwidth in the order of GHz. In general, the main drawback of digital fronthaul is the low bandwidth efficiency, which can be a show stopper for the deployment of wireless fronthaul in future networks.

Since the frequency spectrum is a rare and expensive asset, mobile operators have to consider bandwidth efficiency as a key figure of merit for wireless technologies. Therefore, a new wireless fronthaul concept is presented in paper [F] as a potential enabler for cost efficient and scalable fronthaul networks. The basic idea is to carry narrow band analog radio access signals over millimeter-wave frequency instead of being transported using multi-gigabit digital CPRI. The analog wireless fronthaul is much more bandwidth efficient than the conventional digital wireless fronthaul.

The link implementation of the analog fronthaul is different compared to that of the digital fronthaul. The main functional blocks are outlined in Fig. 4.5. The digital wireless fronthaul is a replacement of the optical fiber and equipped with CPRI interface, where the digital radio signals (I/Q samples) are modulated on mm-wave carriers. However, the analog fronthaul relays analog radio signals over mm-wave carriers between the centralized BBU and RRUs. Taking the downlink as an example, digital radio signals are generated at the BBU, and the analog fronthaul converts the signals to analog format which are then up-converted to mm-wave and transmitted over the air. At the cell site, received signals are first down converted from mm-wave to radio frequency (RF) and then amplified to communicate with user terminals. Therefore, the RRU is simplified to contain only the mm-wave front-end for frequency up/down conversion and RF amplifiers. The power hungry data converters (DAC/ADC) are no longer needed, which further reduces the site power consumption in the centralized baseband networks.

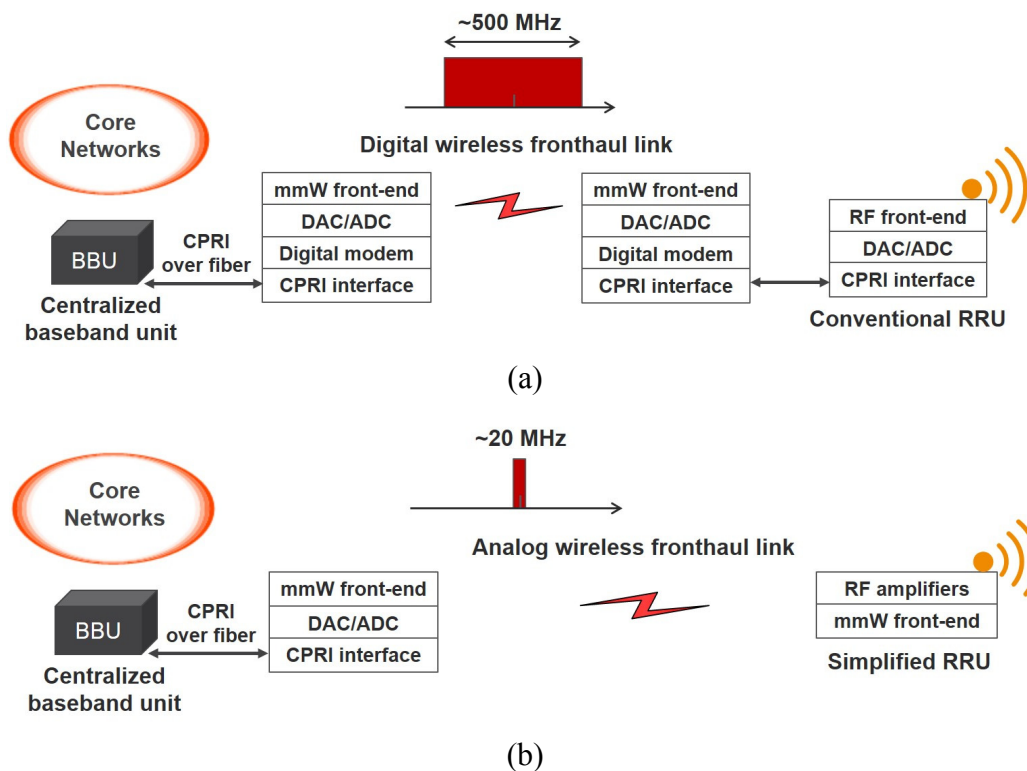


Figure 4.5: Comparison of end-to-end fronthaul link implementations, (a) digital wireless fronthaul, and (b) analog wireless fronthaul [F].

4.2.1 Advantages and challenges

Digital fronthaul even using spectrally efficient modulation (e.g. 64-QAM) requires at least a few hundreds of MHz bandwidth for 2.5 Gbps CPRI transmission to support one LTE sector. Instead, the analog fronthaul links only carry the corresponding LTE radio signals in 20 MHz over the air. Since the required bandwidth of CPRI transmission is much higher than the bandwidth of the actual radio signals, digital fronthaul is not appropriate to support multi sectors and MIMO for capacity upgrade in future mobile networks. The analog fronthaul, however, as a bandwidth efficient solution, is data-rate scalable by frequency multiplexing narrow band radio signals onto a mm-wave carrier. Moreover, the analog fronthaul allows simultaneous transport of multiple radio access services (e.g. 2G/3G/4G/WiFi) due to transmission of analog radio signals, while the digital CPRI transmission typically only supports one service at a time. Fig. 4.6 illustrates the deployment of small cells using remote radios from a macro site to enhance capacity and coverage. Analog radio signals are generated at the macro site and transmitted to RRUs through analog fronthaul links using point-to-point or point-to-multipoint connection. Each RRU supported by the analog fronthaul can be configured for one specific service or multi-service. For the RRUs not situated in line-of-sight relative to the macro radio base station (e.g. RRU4 in Fig. 4.6), the fronthaul connection is established by using the mm-wave carrier to distribute radio signals through line-of-sight links in a daisy chain fashion.

Despite cost and performance advantages of the analog fronthaul, there are also technical challenges to overcome. Since it is analog radio signals that are transmitted rather than digital signals, high linearity is required for the analog links. For short links of few hundred meters,

the radio transmitters can operate in the linear region due to the relatively high gain of the mm-wave antennas. However, nonlinearity compensation of the amplifiers should be considered to improve system gain for longer transmission links and/or better reliability. The concept of analog fronthaul can be realized at RF, microwave and millimeter-wave frequencies. Millimeter-wave is more attractive with a large bandwidth available for carrier aggregation to enable high link capacity. In addition, it reduces cost for operators to deploy mm-wave links using license free 60 GHz band or light licenced 70/80 GHz (E-band). However, radio impairments such as phase noise and frequency error also increase proportionally to the carrier frequency. For example, phase noise increases as much as 30 dB when the carrier frequency is shifted from 2.6 GHz to 80 GHz. The baseband digital signal processing in conventional radio base stations and user terminals is not capable of handling high frequency noise as such. Thus, the added signal noise over the mm-wave fronthaul link must be minimized to maintain the performance of the radio access signals, so that users do not experience any service degradation.

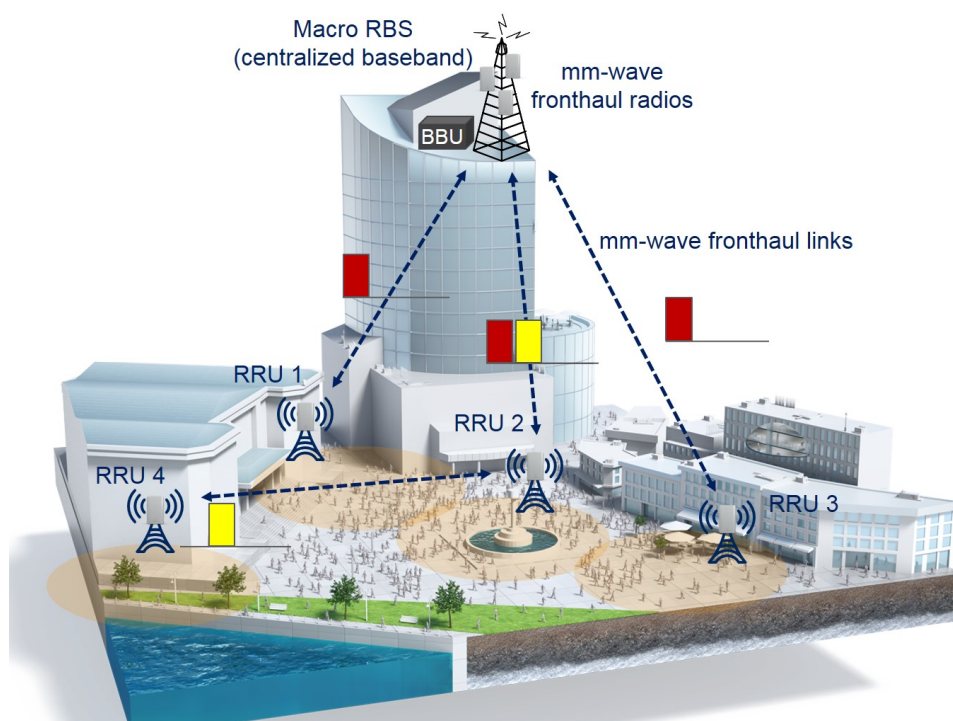


Figure 4.6: Deployment of analog mm-wave fronthaul links from/to a macro site [F], where different RRUs could use different sub-bands.

4.3 High frequency impairments mitigation

An analog phase noise mitigation method has been proposed for mm-wave systems in paper [E]. It uses an RF pilot as a phase reference to cancel both phase and frequency impairments of an arbitrary mm-wave signal at the expense of pilot bandwidth overhead. The method is verified experimentally at carrier frequency of 28 GHz and at 73 GHz (E-band), showing a significant noise reduction within the 100 kHz offset.

It is technically challenging and costly to realize low phase noise oscillators at high frequencies. The analog phase noise mitigation method is attractive to mm-wave systems

since it relaxes the front-end phase noise requirement which lowers the hardware cost. It can also complement digital cancellation to improve transmission performance. More importantly, it can potentially be an enabler using mm-wave for mobile communications (5G), e.g. carrying LTE signals.

4.3.1 The principle of phase noise mitigation

Fig. 4.7 illustrates the concept of analog phase noise mitigation in a heterodyne radio link. A low power RF-pilot tone is added next to an arbitrary signal on the transmitter side at the intermediate frequency (IF) stage. The pilot tone is co-transmitted with the data signal over a mm-wave channel so that it is distorted in the same way as the signal by phase noise and frequency offset due to frequency up and down conversion at mm-wave domain. Hence, the pilot can be used as a phase reference at the receiver side to restore the signal by noise cancellation using frequency multiplication.

There are different ways to place the pilot, in the middle of the signal spectrum [25] or next to the signal with a small frequency separation [26]. Inserting a pilot in the middle of the signal does not consume extra bandwidth, but it limits the system flexibility not to allow arbitrary signal transmission. Moreover, a pilot on top of the signal spectrum requires a reduced transmitter output power in order to fulfil the spectrum mask requirement for commercial radio systems, and it is thus of less practical interest.

One possible receiver implementation for phase noise mitigation is depicted in Fig. 4.7 (b). The received signal is first down converted from mm-wave to IF frequency f_I , and split into two branches. The pilot is selected by a narrow band pass filter (BPF), and then multiplied with the signal using a frequency mixer. At the mixer output, the phase and frequency impairments introduced over the mm-wave are cancelled for the down converted signal at f_{IF-f_p} , while the image frequency f_{IF+f_p} carries doubled impairments due to noise addition. As long as $2*f_p$ is larger than the bandwidth of the signal plus the small pilot frequency separation, the image frequency will not overlap with the wanted signal and can be removed by a filter or simply using a single sideband mixer. In practical receivers, the BPF-induced delay should be properly matched in the other branch in front of the mixer for a good performance. Due to conversion loss and other losses, power amplification of the selected pilot is needed to ensure a good dynamic range for the noise reduction. If required by the receiver, the restored signal shall be converted back to the original frequency f_{IF} by an additional frequency conversion.

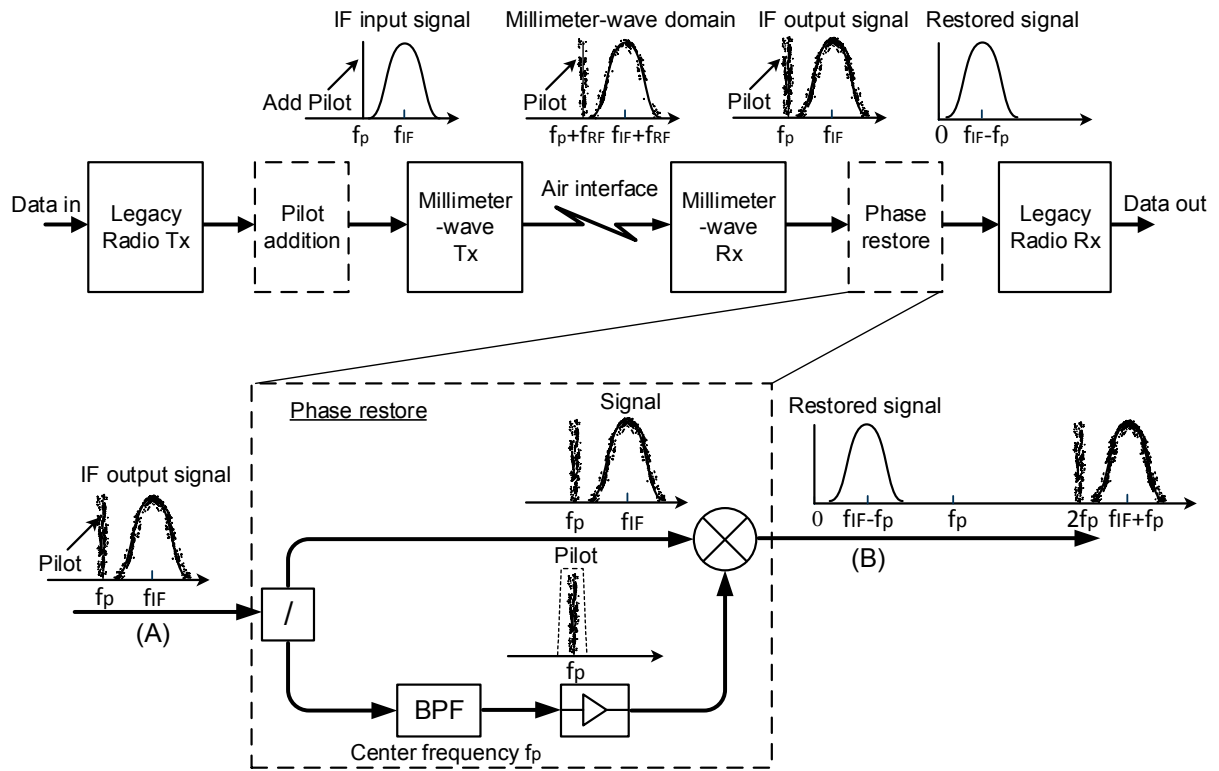


Figure 4.7: Pilot-based phase noise mitigation in a heterodyne millimeter-wave radio link, and one possible receiver implementation of the phase-restore process [E].

4.3.2 Performance optimization

There are two critical parameters to optimize in the pilot-based mitigation for system performance: the bandwidth of the BPF for selecting the pilot and the pilot-to-signal power ratio (PSPR) [E]. The BPF bandwidth has an impact on the degree of phase noise reduction, since the pilot tracks the signal phase up to a frequency offset defined by the filter bandwidth. As reported in [25], the optimum filter bandwidth depends on the given phase noise figure of the oscillator. Higher phase noise increases the spectrum spreading of the pilot, and thus a wider filter is needed to select the complete pilot. However, to save bandwidth, a pilot shall be placed as closely as possible to the signal spectrum and the filter, as a result, shall be relatively narrow. In practice, the chosen filter bandwidth is a trade-off between spectral efficiency and phase noise performance.

The power of the pilot tone should also be optimized. The pilot power shall be low due to the transmitter output power constraint from the power mask requirement. However, it can not be too weak so that the SNR of the pilot limits the degree of phase noise reduction. In practical transmitters, the pilot should be implemented with automatic gain control to compensate for the gain variation in a frequency selective radio channel.

4.3.3 Experimental demonstration over millimeter-wave

As a proof-of-concept demonstration, experiments are carried out at both 28 GHz and at 73 GHz (E-band) using commercial microwave components and millimeter-wave transceiver modules, as shown by the photo in Fig. 4.8. In the measurement, a sinusoidal signal is transmitted as the carrier signal without modulated data in order to directly measure phase noise improvement using a spectrum analyzer.

Phase noise of the carrier signal is first measured at the output of the mm-wave Rx at f_{IF} (point A in Fig. 4.7), and then is measured again at the output of the noise mitigation mixer (point B in Fig. 4.7). The results are displayed in Fig. 4.9 as a comparison of before and after the mitigation, where phase noise is presented in dBc/Hz vs. frequency offset from the carrier. In both experiments at 28 GHz and the E-band, the pilot-based mitigation method demonstrates more than 20 dB noise reduction within the 100 kHz offset and more than 30 dB reduction at 10 kHz offset. However, as shown in Fig. 4.9 (a), the mitigated phase noise starts to saturate beyond 100 kHz due to poor SNR of the measured carrier signal that limits the noise reduction. A similar result is also measured at E-band (Fig. 4.9 (b)).

The first experimental set-up aims to prove the noise mitigation concept with loose requirements on spectral efficiency and component performance. For instance, the BPF is chosen upon hardware availability, and the bandwidth is not optimized for the given phase noise figure. Requirements of the BPF and the impact of pilot-to-signal separation and pilot-to-signal power ratio on system performance shall be further investigated.

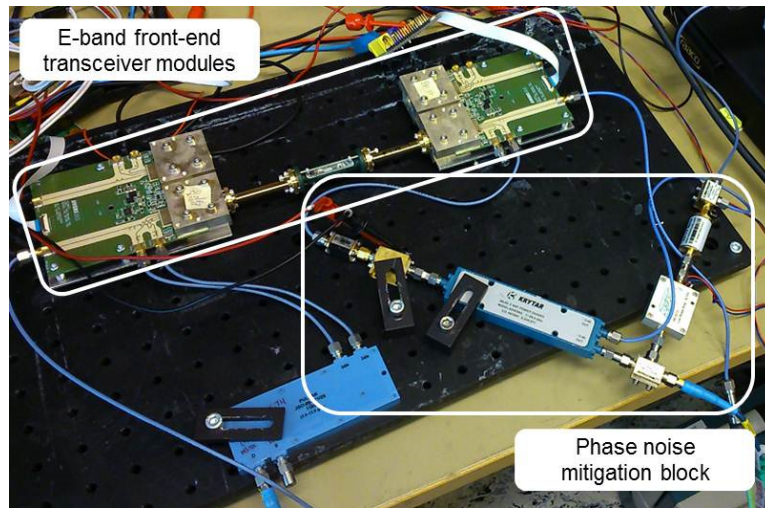
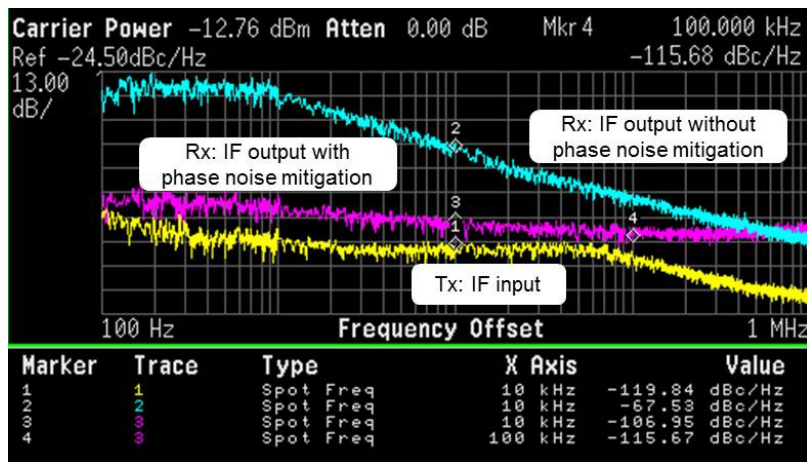
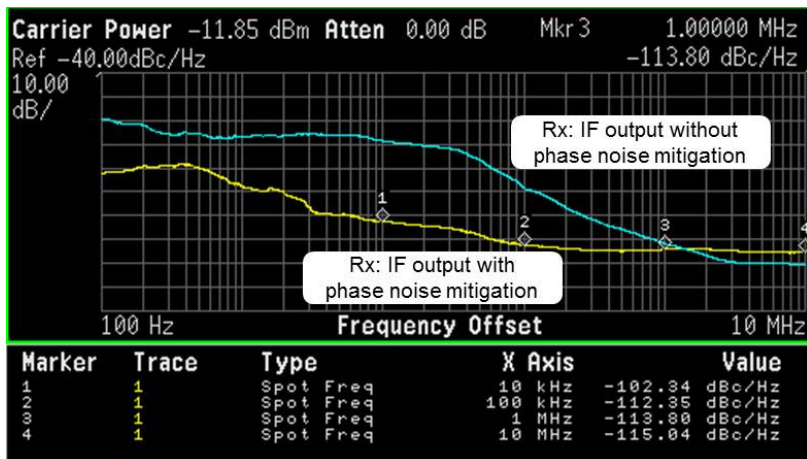


Figure 4.8: Measurement set-up for the pilot-based mitigation over E-band [E].



(a)



(b)

Figure 4.9: Measured phase noise of the received IF carrier signal before and after the pilot-based phase noise mitigation (a) over the 28 GHz band, and (b) over E-band at 73 GHz [E].

4.4 Analog fronthaul demonstrator

To demonstrate the feasibility of analog mm-wave fronthaul, a test link is designed and implemented at 70/80 GHz (E-band) with pilot-based phase noise mitigation applied to restore the signal at the receiver [E]. Thanks to the noise mitigation, 20 MHz 64-QAM LTE uplink and downlink transmission is demonstrated over E-band with measured error vector magnitude (EVM) of about 3% at the expense of 10% pilot bandwidth overhead. Moreover, the impact of the pilot overhead and the pilot signal strength on transmission performance is also investigated.

4.4.1 Implementation of analog fronthaul at 70/80 GHz

The analog fronthaul link is implemented using commercial RF components and mm-wave front-end modules, as shown by the photo in Fig. 4.10. The LTE uplink and downlink signals are generated from a vector signal generator, with 20 MHz bandwidth and 64-QAM modulation format. The signal quality is evaluated in a signal analyzer, which demodulates the LTE signals digitally and measures the EVM as performance indicator.

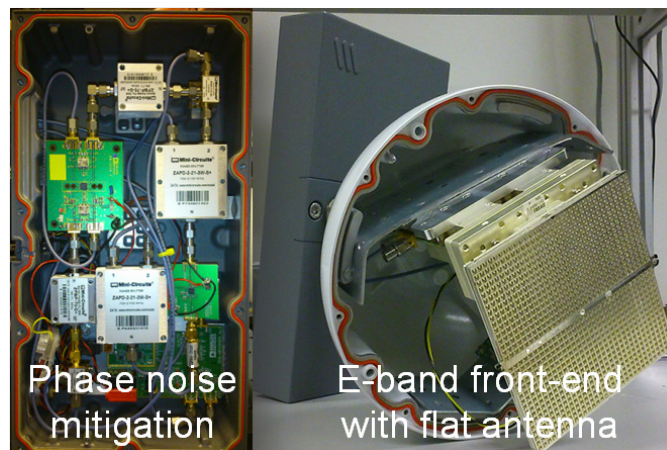


Figure 4.10: Photo of one analog fronthaul radio.

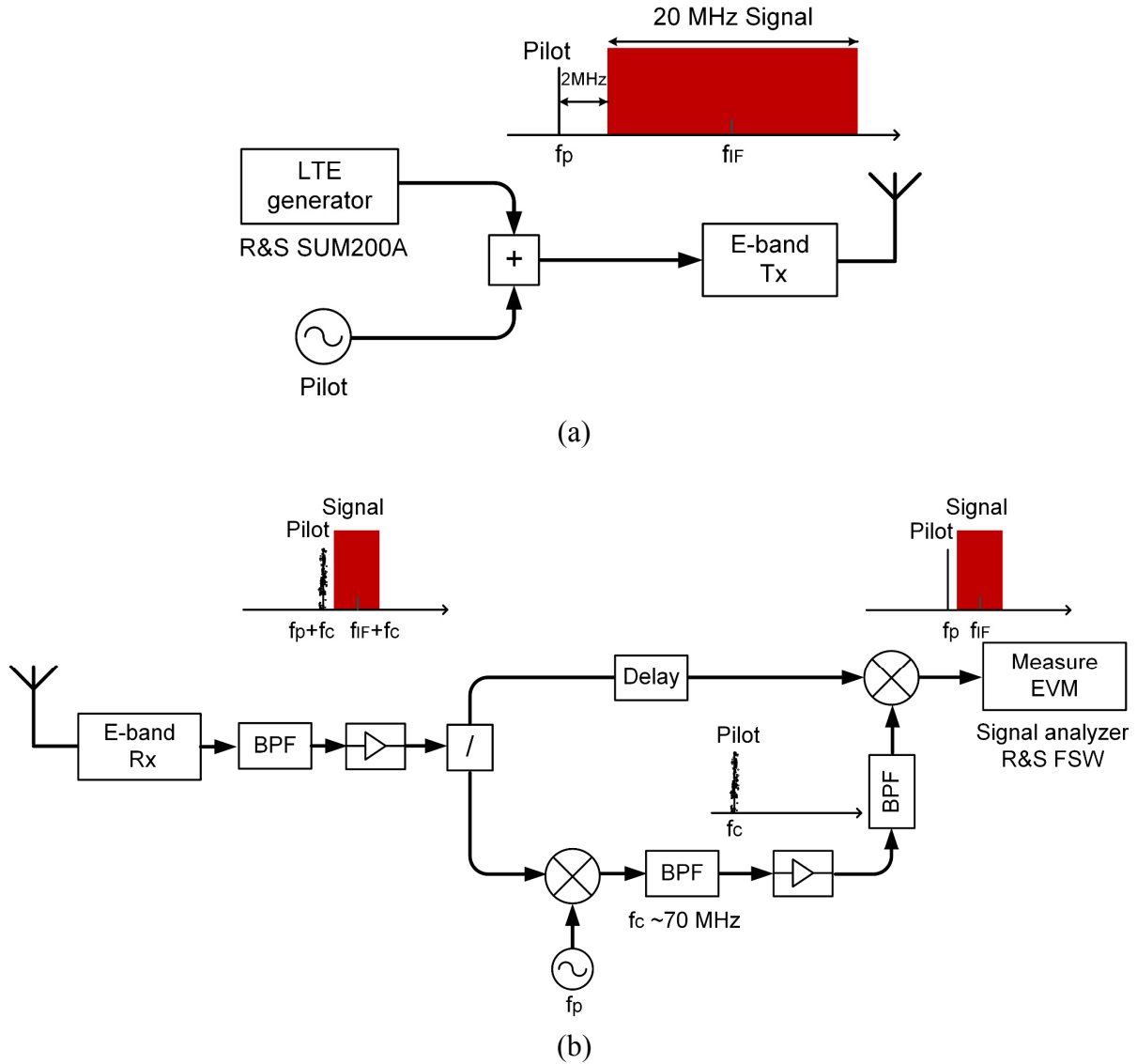


Figure 4.11: Experimental set-up of the analog fronthaul link, (a) transmitter with an RF-pilot added, and (b) receiver with the pilot-based phase noise mitigation [F].


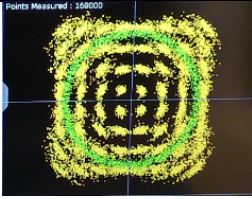

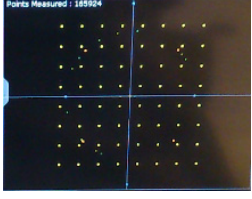
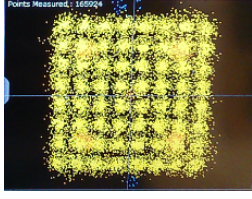

Fig. 4.11 presents the block diagram of the fronthaul link set-up. At the transmitter side, a sinusoidal wave as the pilot tone (f_P) is added next to the LTE signal centered around 1.8 GHz (f_{IF}) by a power combiner. The frequency separation between the pilot and the signal spectrum is 2 MHz, as indicated in Fig. 4.11 (a). The pilot power is 10 dB lower than the signal power. The combined pilot and LTE signal are up converted to E-band low band at 73 GHz. In the laboratory experiment, the E-band Tx and Rx are connected through a waveguide attenuator and without antennas, and the value of attenuation is adjustable. On the receiver side, the pilot and the signal are first down converted to the IF stage. The pilot is selected after a second frequency down conversion using a band pass filter (BPF) with 2 MHz bandwidth and centered at 70 MHz (f_c).

4.4.2 Evaluation of transmission performance

To evaluate the performance of LTE transmission over E-band, signal EVM is measured at the transmitter and the receiver, respectively. The results are summarized in Table V together

with captured constellation diagrams. The quality of the LTE signal directly from the generator is very high with EVM below 1%. The signal is distorted by phase noise due to frequency up and down conversion at E-band and the EVM is degraded and is larger than 10%. The pilot-based noise mitigation restore the signal with EVM of about 3%, well below the EVM requirement of 8% for 64-QAM as defined in the 3GPP technical specification [27]. Fig. 4.12 is a screen shot of a spectrum analyzer showing the pilot next to the 20 MHz LTE signal, where the pilot is 2 MHz separated from the signal spectrum with 10 dB lower in power. The effect of phase noise on transmission performance is similar for both uplink and downlink as indicated with the measured EVM values. However, the phase noise impact on signal constellation is different between uplink and downlink due to the inherent difference in the signal construction. The uplink signal is more sensitive to the common phase error which rotates the constellation diagram, while inter-carrier interference is dominant in the downlink shown as enlarged constellation points [28].

Table V: Measured signal quality for 64-QAM LTE uplink and downlink over 73 GHz carrier [F].

	Signal input to E-band at f_{IF}	Signal over E-band at $f_{IF} + f_c$	Signal after mitigation at f_{IF}
20 MHz LTE uplink			
EVM	<1%	~11%	~3%
20 MHz LTE downlink			
EVM	<1%	~12%	~3%

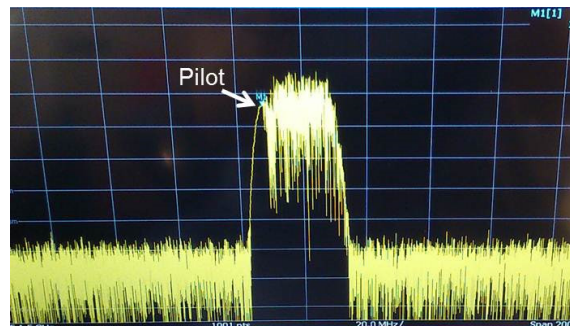


Figure 4.12: A screen photo showing the combined pilot and 20 MHz LTE signal in a spectrum analyzer with 3 MHz resolution bandwidth and 200 MHz span.

For the designed fronthaul link, a BPF with 2 MHz bandwidth is chosen as an acceptable trade-off between system spectral efficiency and performance. To avoid cross-talk between the signal and the pilot, the required frequency separation between the pilot and the signal spectrum (pilot-signal separation) is optimized. We have also optimized the pilot-to-signal power ratio (PSPR) with respect to the signal performance measured after the noise mitigation. Since the pilot is generated from a signal generator, the pilot frequency and the power strength can easily be tuned.

The impact of the pilot-signal spectrum separation on signal EVM for the LTE downlink is shown in Fig. 4.13. Four measured curves represent different PSPR values from -4 dB to -13 dB with 3 dB as a step. For instance, PSPR -4 dB means the pilot power is 4 dB lower than the total signal power. It is clear that all the curves demonstrate the same trend where the EVM is significantly reduced with an increased pilot-signal separation from 2 MHz to 4 MHz. Besides, increasing the pilot power also helps to improve the performance, which is obvious from the difference between the curve of PSPR -13 dB and the one of PSPR -10 dB. However, the improvement is minor with further increased pilot power due to performance saturation of the phase noise mitigation. Considering the trade-offs between performance and spectral/power efficiency, pilot-signal separation of 4 MHz and PSPR of -10 dB are chosen for the fronthaul link characterization.

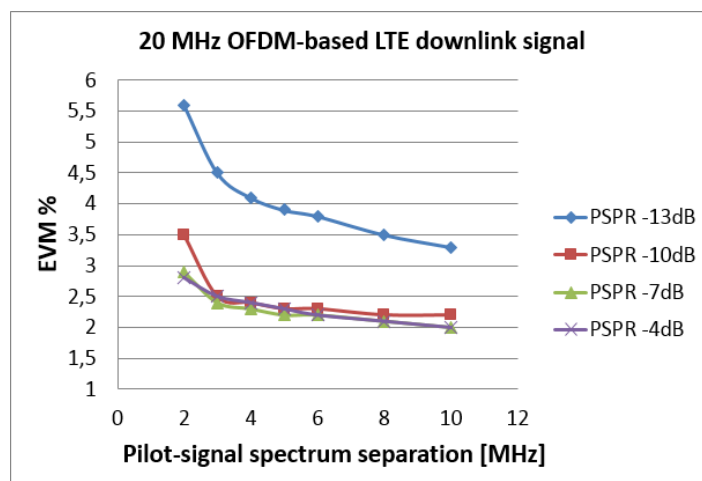


Figure 4.13: Impact of pilot-signal separation on signal quality in terms of measured EVM at different pilot power levels [F].

4.4.3 Fronthaul link characterization

Receiver sensitivity

The fronthaul link is characterized using a 20 MHz OFDM-based LTE downlink signal in frequency division duplex scheme over E-band, where the low band is centered at 73 GHz and the high band is centered at 83 GHz. The input signal power to the E-band Rx is adjustable by varying the attenuation between the radio transmitter and the receiver. Signal quality after the noise mitigation is measured as a function of the varied Rx input power, as displayed in Fig. 4.14. Assuming EVM of 3% as the performance threshold, Rx sensitivity is measured to be -53 dBm for E-band low band and -51 dBm for the high band. The difference in sensitivity is due to the 2 dB higher in noise figure for the high band Rx module.

Comparing with theoretical calculation of receiver sensitivity in [29], the fronthaul test link has a 3 dB implementation loss.

Receiver dynamic range

The rapid performance degradation in Fig. 4.14 at high input power is caused by the nonlinear effect of the commercial E-band Rx. In addition to improving linearity of the front-end circuits, such as the amplifier and the mixer, including automatic gain control in the receiver can also help to prevent overloading and thus increase the receiver dynamic range.

System gain

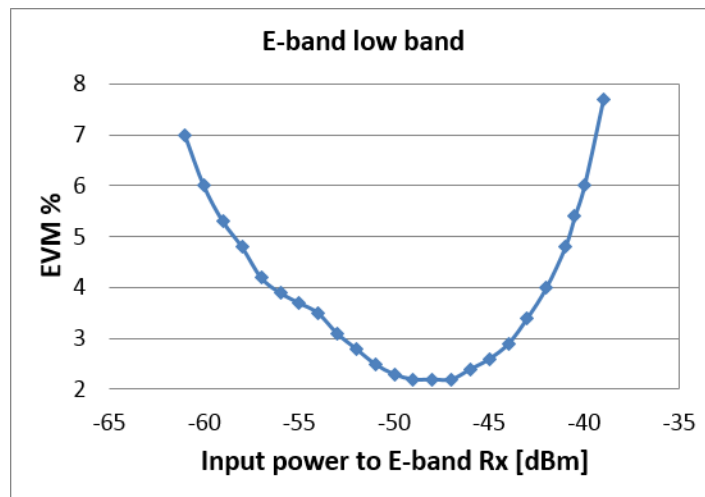
To have an estimation of the maximum fronthaul link distance for the given implementation, system gain is calculated in Table VI for the E-band low band transmission using the following equation:

System gain (dB) = Tx output power (dBm) + Tx antenna gain (dBi) + Rx antenna gain (dBi) – Rx sensitivity (dBm).

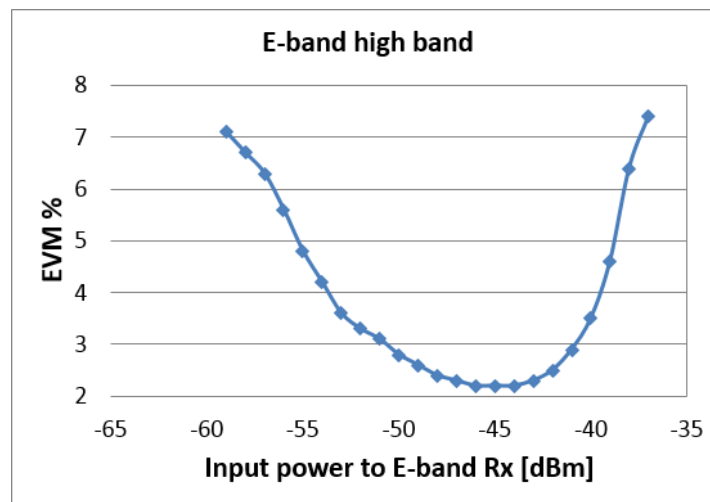
Sufficient margin is always needed to account for fading, which is mainly the rain attenuation for line-of-sight point-to-point radio links. In a scenario of using the fronthaul links to deploy small cells for capacity within an existing macro area, a fading margin of 10 dB is required for 99.9% availability [30]. Thus, the fronthaul link is limited to 500 meters. To improve link distance and/or availability, the easiest way is to use bigger antennas with more gain (e.g. 43 dBi instead of 38 dBi that we have used). Besides, the Tx output power can also be increased by complementing the front-end with some linearization technique.

Table VI: Link budget analysis for the analog fronthaul demonstrator.

Tx output power	5 dBm
Tx/Rx antenna gain (dBi)	38 dBi
Rx sensitivity for 3% EVM	-53 dBm
System gain	134 dB
Link margin	10 dB
Link distance	0.5 km



(a)



(b)

Figure 4.14: Measured EVM of the LTE downlink signal as a function of input power to the E-band Rx, (a) for E-band low band, and (b) for E-band high band [F].

Chapter 5

Conclusions and Future Outlook

5.1 Conclusions

This thesis presents modem and system implementations for multi-gigabit radio transmission in next generation mobile networks. Taking the advantage of large bandwidth at millimeter-wave frequency bands, it is feasible to realize multi-gigabit capacity in spite of challenges associated to wide signal bandwidth and radio impairments at high carrier frequency. The presented solutions address the challenges and demonstrate the feasibility using commercially available hardware. The 70/80 GHz (E-band) has been the target frequency band for the performance evaluation and system prototyping, which offers a total bandwidth of 10 GHz and is regulated worldwide for commercial use with light licensing.

The global mobile data explosion has been driving the evolvement of mobile networks from 3G to 4G and the development will continue into 5G and beyond. As a consequence, the capacity of mobile backhaul networks has to be increased, specifically for the capacity of the dominant technology, microwave transmission. By utilizing wide bandwidth design, 2.5 Gbps and 5 Gbps DQPSK modems are implemented without high speed data converters aiming to cost- and power-efficient system applications. We take the next step to further increase the capacity by applying higher order modulation formats. A 16-QAM baseband demodulator is realized in a hardware efficient manner using an analog design to complement a digital modem. As a result, the achieved data rate goes beyond what had been possible while the sampling rate of the ADC was the limitation. On the other hand, for the same data rate a lower-end ADC might be used as an option to reduce cost and power consumption. Based on the demodulator, a 5 Gbps radio system is demonstrated at 70/80 GHz band.

The realization of multi-gigabit radio transmission also opens up opportunities for wireless fronthaul links in the centralized baseband architecture, which is an attractive solution to support the network densification for capacity and coverage enhancement. A data-rate adaptable modem solution is proposed for wireless digital fronthaul systems using millimeter-wave bands. The modem is verified at data rates up to 10 Gbps, and fulfils the CPRI specifications. As an alternative, an analog fronthaul technology is introduced. It greatly improves the bandwidth efficiency as opposed to the digital fronthaul, and it is therefore flexible for capacity upgrades of fronthaul networks. The analog fronthaul is demonstrated at 70/80 GHz band complemented with analog phase noise mitigation. 64-QAM LTE transmission is achieved over the fronthaul link with marginal performance impact, compared to commercial LTE systems at cellular bands.

Considering system complexity and hardware limitations, the solutions in the thesis achieve multi-gigabit capacity utilizing wide bandwidth designs and relatively simple structures. Due to the high symbol rate of such systems, it is challenging to apply digital modulation. Therefore, analog implementations are show-cased in DQPSK and the 16-QAM modems with the benefits of low cost and low power consumption. The benefit of using analog signal processing is shown in the fronthaul demonstrator that it efficiently reduces phase noise induced at the high carrier frequency.

5.2 Opportunities at 140-GHz band

Multi-gigabit millimetre-wave radio is a cost efficient and flexible alternative to optical fiber communication. However, the capacity of deployed optical links has been increased from 10 Gbps to 40 Gbps and even 100 Gbps is commercially available. To be future proof and fiber competitive, capacity evolution of the millimetre-wave radio transmission will continue aiming at higher capacity at higher frequency bands.

The next atmospheric window beyond 70/80 GHz band is the 140-GHz band, allocated from 141 – 148.5 GHz. The 140-GHz band has gained research interest because it is possible to reach km-transmission based on current hardware technologies and the band is regulated for fixed services. A world record of 40 Gbps is demonstrated at microwave electronic laboratory, Chalmers University of Technology [31].

Aiming at 100 Gbps transmission over the 140-GHz band, a spectrally efficient modulation shall be employed. However, the modulation order is determined by the SNR of the system. The SNR can be estimated in circuit-design phase by system simulation. Moreover, simulation offers the possibility to optimize the SNR by performance coordination among key functional blocks and function partitioning between analog and digital domains. Therefore, it is crucial to perform system level study for the implementation of radio systems towards 100 Gbps.

Acknowledgments

In June 2007, I defended my master thesis work at MC2. By then I thought it was a beautiful ending to my life period as a student. Obviously, I am not always right but I am very happy that I decided to continue the journey.

So, taking the opportunity I would like to express my deep gratitude to all the people who made this work happen.

First of all, I would like to say thank you to my previous manager Dr. Thomas Lewin for giving me the opportunity to work at Ericsson Research and start my life in Gothenburg. It was his trust that encouraged me to take the challenge of pursuing a PhD study. Also, I am very grateful to my examiner (and colleague) Prof. Herbert Zirath for taking me as a PhD student and his support on my study in all possible ways. In addition, special thanks go to Associate Prof. Thomas Swahn as my supervisor for many inspiring discussions and concrete feedbacks on my papers and thesis writing. More importantly, his positive attitude cheered me up when I was at the low point several times. I also appreciate the guidance from Prof. Christer Svensson and his considerable contributions to the ‘MODEM’ project.

I want to thank all my close colleagues at Ericsson Research for being supportive on my work and study. It is them who make me feel so lucky and proud of working at Ericsson. Especially, I am grateful to Dr. Yinggang Li, Dr. Jonas Hansryd and Dr. Bengt-Erik Olsson for teaching me a lot! Besides, I am thankful to Dr. Zhongxia He for being a wonderful colleague. It was with him that I spent most of the time in the lab. It would not be possible to present these many results without his help.

I want to thank my friends (at the same time colleagues), Lei, Tingting, Samuel and Martin for being so kind and making my life easy. I also want to thank Thomas for his encouragement and all the fun games that we have had.

Finally, I would like to thank my parents for their unconditional love and faith in me. I am very grateful to my close friend Zonghe, who has always been there for me. I could not have reached this far without him. I want to say thank you to Géza for bringing me so many interesting moments and good comments on my writing.

This work has been financially supported by VINNOVA ‘MODEM’ project, SSF project ‘system on chip solutions for future wireless high speed communication applications’, and Ericsson Research, Ericsson AB.

References

- [1] “Cisco Visual Networking Index: Global Mobile Data Traffic Forecast Update, 2013–2018”, <http://www.cisco.com>, February, 2014.
- [2] Ericsson mobility report June 2014. <http://www.ericsson.com/res/docs/2014/ericsson-mobility-report-june-2014.pdf>.
- [3] E. Dahlman, G. Mildh, S. Parkvall, J. Peisa, J. Sachs, Y. Selen, 5G radio access, Ericsson Review, June, 2014.
http://www.ericsson.com/res/thecompany/docs/publications/ericsson_review/2014/er-5g-radio-access.pdf.
- [4] J. Hansryd, P-E Eriksson, High-speed mobile backhaul demonstrators, Ericsson Review, February, 2009. http://www.ericsson.com/ericsson/corpinfo/publications/review/2009_02/files/Backhaul.pdf.
- [5] China mobile research institute, “C-RAN the road towards green RAN,” White paper v. 2.6, Sept., 2013.
- [6] CPRI interface specification, v. 6.0, Aug., 2013.
- [7] 3GPP TS 36.141 v. 9.8.0, “LTE; Evolved Universal Terrestrial Radio Access (EUTRA),” Technical Specification Group Radio Access Network, Rel. 9, July, 2011.
- [8] A. Pizzinat, P. Chanclou, T. Diallo, F. Saliou, “Things you should know about fronthaul,” *European Conference on Optical Communication (ECOC)*, Sept., 2014.
- [9] J. Wells, “Faster than fiber: the future of multi-Gb/s wireless,” *IEEE microwave magazine*, May, 2009.
- [10] J. Hansryd, J. Edstam, “Microwave capacity evolution,” *Ericsson Review*, 1/2011.
- [11] F. Xiong, *Digital Modulation Techniques*, 2nd edition Norwood, USA: Artech House, chapter 9, 2006.
- [12] I. Kallfass et al., “All active MMIC-based wireless communication at 220 GHz,” *IEEE Trans. THz Sci. Technol.*, vol. 1, no. 2, pp. 477–487, Nov., 2011.
- [13] H. -J. Song, K. Ajito, Y. Muramoto, A. Wakatsuki, T. Nagatsuma, and N. Kukutsu, “24 Gbit/s data transmission in 300 GHz band for future terahertz communications,” *Electron. Letters*, vol. 48, no. 15, 2012.
- [14] V. Dyadyuk, J. D. Bunton, J. Pathikulangara, R. Kendall, O. Sevimli, L. Stokes, D. A. Abbott, “A multigigabit millimeter-wave communication system with improved spectral efficiency,” *IEEE Trans. Microw. Theory Techn.*, vol. 55, No. 12, Dec., 2007.
- [15] M. S. Kang, B. S. Kim, K. S. Kim, W. J. Byun and H. C. Park, “16-QAM-Based Highly Spectral-Efficient E-band Communication System with Bit Rate up to 10Gbit/s,” *ETRI Journal*, vol. 34, issue 5, pp. 649-654, October, 2012.
- [16] L. Zhao, H. Shankar, A. Nachum, “40G QPSK and DQPSK modulation,” *Inphi Corporation*.

- [17] R. Gross, "Differential encoder for QPSK systems," *Electronics Letters*, vol. 27, no. 14, 4th July, 1991.
- [18] M. Serbay, C. Wree, W. Rosenkranz, "Implementation of differential precoder for high speed optical transmission," *Electronics Letters*, vol. 40, no. 20, 2004.
- [19] Y. Konishi, K. Ishida, K. Kubo, T. Mizuochi, "True PRBS transmission of DQPSK by differential precoder employing parallel prefix network," *Optical Fiber Communication Conference (OFC' 06)*, pp. 5-10, March, 2006.
- [20] F. Xiong, *Digital Modulation Techniques*, 2nd edition Norwood, USA: Artech House, chapter 4, 2006.
- [21] C. Lin, Q. Chen, B. Lu, X. Deng, and J. Zhang, "A 10-Gbit/s wireless communication link using 16-QAM modulation in 140-GHz band," *IEEE Transactions on Microwave Theory and Techniques*, vol. 61, no. 7, pp. 2733-2746, 2013.
- [22] K. Okada, et al, "A Full Four-Channel 6.3-Gb/s 60-GHz CMOS Transceiver With Low-Power Analog and Digital Baseband Circuitry," *IEEE J. Solid-State Circuits.*, vol.48, no.1, pp.46-65, Jan., 2013.
- [23] A. Hirata, T. Kosugi, H. Takahashi, J. Takeuchi, H. Togo, M. Yaita, N. Kukutsu, K. Aihara, K. Murata, Y. Sato, T. Nagatsuma, and Y. Kado, "120-GHz-band wireless link technologies for outdoor 10-Gbit/s data transmission," *IEEE Trans. Microw. Theory Techn.*, vol. 60, no. 3, pp. 881-895, March, 2012.
- [24] H. Takahashi, T. Kosugi, A. Hirata, K. Murata, N. Kukutsu, "10-Gbit/s QPSK modulator and demodulator for a 120-GHz-band wireless link," *IEEE MTT-S International Microwave Symposium Digest*, pp. 632-635, May, 2010.
- [25] S. L. Jansen, I. Morita, T. C. W. Schenk, N. Takeda, and H. Tanaka, "Coherent optical 25.8-Gb/s OFDM transmission over 4160-km SSMF," *J. Lightw. Technol.*, vol.26, no. 1, pp. 6-15, Jan., 2008.
- [26] B. E. Olsson, C. Larsson, J. Mårtensson, and A. Alping, "Analog electrical phase noise compensation for coherent optical receivers," *ECOC Technical Digest*, Sep., 2012.
- [27] 3GPP TS 36.104 v. 9.4.0, "Base Station (BS) Radio Transmission and Reception," Technical Specification Group Radio Access Network, Rel. 9, July, 2010.
- [28] A. G. Armada, M. Calvo, "Phase noise and sub-carrier spacing effects on the performance of an OFDM communication system," *IEEE Commun. Lett.*, vol. 2, no. 1, pp. 11-13, Jan., 1998.
- [29] David M. Pozar, *Microwave and RF wireless systems*, Wiley, 2001, ch. 10, pp.342.
- [30] Small Cell Forum. "Backhaul Technologies for Small Cells – Use Cases, Requirements and Solutions", Doc. 049.01.01, Feb., 2013.
- [31] S. Carpenter, Z. He, M. Bao, H. Zirath, "A highly integrated chipset for 40 Gbps wireless D-band communication based on a 250nm InP DHBT technology," *IEEE Compound Semiconductor Integrated Circuit Symposium (CSICs)*, Oct., 2014.

Paper A

A novel FPGA-based 2.5Gbps DQPSK modem for high capacity microwave radios

Z. He, **J. Chen**, Y. Li, H. Zirath

International Conference of Communications (ICC2010), Cape Town, May, 2010.

Paper B

10 Gbps 16QAM transmission over a 70/80 GHz (E-band) radio test-bed

J. Chen, Z. He, L. Bao, C. Svensson, Y. Li, S. Gunnarsson, C. Stojj, H. Zirath

European microwave conference (EuMC), Amsterdam, October, 2012.

Paper C

A hardware efficient implementation of a digital baseband receiver for high capacity millimeter-wave radios

Z. He, **J. Chen**, C. Svensson, L. Bao, A. Rhodin, Y. Li, J. An, H. Zirath

Accepted for publication in *IEEE Transactions on Microwave Theory and Techniques*.

Paper D

A data-rate adaptable modem solution for millimeter-wave wireless fronthaul networks

J. Chen, Z. He, Y. Li, T. Swahn, H. Zirath

International Conference of Communications (ICC2015) Workshop, London, June, 2015.

Paper E

Experimental demonstration of RF pilot-based phase noise mitigation for millimeter-wave systems

J. Chen, B. E. Olsson, A. Persson, J. Hansryd

Vehicular Technology Conference (VTC2014-Fall), Vancouver, September, 2014.

Paper F

Demonstration of analog millimeter-wave fronthaul for 64-QAM LTE transmission

J. Chen, B. E. Olsson, J. Hansryd, I. Gerszberg

Submitted to *Vehicular Technology Conference (VTC2015-Fall)*, Boston, September, 2015.

